CONF-951202--4

DEVELOPMENT AND TESTING OF VANADIUM ALLOYS FOR FUSION APPLICATIONS*

by ANL/ET/CP--88143

H. M. Chung, B. A. Loomis, and D. L. Smith

Argonne National Laboratory
Argonne, IL 60439

RECEIVED
NOV 05 1996
OSTI

The submitted manuscript has been created by the University of Chicago as Operator of Argonne National Laboratory ("Argonne") under Contract No. W-31-109-ENG-38 with the U.S. Department of Energy. The U.S. Government retains for itself, and others acting on its behalf, a paid-up, nonexclusive, irrevocable worldwide license in said article to reproduce, prepare derivative works, distribute copies to the public, and perform publicly and display publicly, by or on behalf of the Government.

October 1996

MASTER

To be published in Journal of Nucl. Material (as Proc. International Symposium on Advanced Materials and Technology for the 21st Century, Honolulu, Hawaii, December 13–15, 1995)

*Work supported by the U.S. Deaprtment of Energy, Office of Energy Research.

DISTRIBUTION OF THIS DOCUMENT IS UNLIMITED

DISCLAIMER

Portions of this document may be illegible in electronic image products. Images are produced from the best available original document.

DISCLAIMER

This report was prepared as an account of work sponsored by an agency of the United States Government. Neither the United States Government nor any agency thereof, nor any of their employees, makes any warranty, express or implied, or assumes any legal liability or responsibility for the accuracy, completeness, or usefulness of any information, apparatus, product, or process disclosed, or represents that its use would not infringe privately owned rights. Reference herein to any specific commercial product, process, or service by trade name, trademark, manufacturer, or otherwise does not necessarily constitute or imply its endorsement, recommendation, or favoring by the United States Government or any agency thereof. The views and opinions of authors expressed herein do not necessarily state or reflect those of the United States Government or any agency thereof.

DEVELOPMENT AND TESTING OF VANADIUM ALLOYS FOR FUSION APPLICATIONS*

H. M. Chung, B. A. Loomis, and D. L. Smith
Argonne National Laboratory
Argonne, IL 60439, U.S.A.

Abstract

Vanadium-base alloys are promising candidate materials for application in fusion reactor first-wall and blanket structure because of several important advantages, i.e., inherently low irradiation-induced activity, good mechanical properties, good compatibility with lithium, high thermal conductivity, and good resistance to irradiation-induced swelling and damage. To screen candidate alloys and develop an optimized vanadium-base alloy, extensive investigations of physical and mechanical properties of various V-Ti, V-Cr-Ti, and V-Ti-Si alloys have been conducted before and after irradiation in lithium environment in fast fission reactors. From these investigations, a V-4Cr-4Ti alloy containing 500-1,000 wppm Si and <1,000 wppm O+N+C has been identified as the most promising alloy, and more comprehensive testing on the performance of this alloy is being conducted for fusion-relevant conditions. Major results of the comprehensive work to develop the optimal alloy and test the irradiation performance are presented in this paper. The reference alloy V-4Cr-4Ti exhibited the most attractive combination of the mechanical and physical properties that are prerequisite for first-wall and blanket structures, i.e., good thermal creep behavior, good tensile strength and ductility, high impact energy, excellent resistance to swelling, and very low ductile-brittle transition temperature before and after irradiation. The alloy was highly resistant to irradiation-induced embrittlement in Li at 420–600°C, and the effects of dynamically charged helium on swelling and mechanical properties were insignificant. However, several important issues remain unresolved, e.g., welding, low-temperature irradiation properties, helium effect at high dose and high helium concentration, irradiation creep, and irradiation performance in air or helium environment. Initial results of investigation of some of these issues are also given.

1. Introduction

Development of a good structural material is one of the most important tasks in the extensive international efforts aimed to harness fusion energy and develop a working fusion power reactor. Ideally, such a material should exhibit attractive characteristics such as low induced activation, good tolerance to high operating temperature and stress, long-term reliability under operating conditions, good fabricability and weldability, and reasonable production cost. Vanadium-base alloys have been recognized for many years as having significant advantages for use as structural materials in magnetic fusion reactors. These advantages include intrinsically lower levels of long-term activation, irradiation afterheat, neutron-induced helium- and hydrogen-transmutation rates, biological hazard potential, and thermal stress factor.[1–5] However, to make use of these favorable neutronic and physical properties of vanadium-base alloys in fusion systems, it must be demonstrated that the alloys are resistant to neutron-induced swelling, creep, and embrittlement, and also compatible with the reactor coolant and expected operational transients. The industrial base of vanadium alloy fabrication is rather limited and there is no previous experience in other energy systems such as light-water or fast-breeder reactors; therefore, it must be also demonstrated that the alloy(s) can be produced, fabricated, and welded to form large-scale field components in a reliable manner.

2. Alloy Fabrication

A large number of V–Cr and V–Ti binary and V–Cr–Ti and V–Ti–Si ternary alloys were fabricated at laboratory scale (15–30 kg) and investigated in this program. The elemental composition of the alloys is given in Table 1. Typically, a small ingot was vacuum-arc-

*Work supported by the U.S. Department of Energy, Office of Fusion Energy, under Contract W-31-109-Eng-38.

-melted using electron-beam-melted vanadium raw stock and high-purity double- or triple-arc-melted Ti. The ingot was extruded at 1150°C and annealed at 1050°C several times after 8–10 passes of cold- or warm-rolling (at ≈400°C) between the annealings.

Table 1. Composition of vanadium-base alloys investigated

	Nominal Comp.	Impurity Concentration (wt. ppm)			
Heat ID	(wt.%)	O	N	C	Si
BL-19	V	1101	161	360	–
BL-20	V	570	110	120	325
BL-36	V	810	86	250	<50
BL-51	V	570	49	56	370
820626	V	260	75	28	260
820630	V	200	62	75	780
BL-35	9.5Cr	340	45	120	<50
BL-4	10.0Cr	530	76	240	<50
BL-5	14.1Cr	330	69	200	<50
BL-50	1.0Ti	230	130	235	1050
BL-52	3.1Ti	210	310	300	500
BL-46	4.6Ti	305	53	85	160
BL-11	4.9Ti	1820	530	470	220
BL-34	8.6Ti	990	180	420	290
BL-12	9.8Ti	1670	390	450	245
BL-13	14.4Ti	1580	370	440	205
BL-15	17.7Ti	830	160	380	480
BL-16	20.4Ti	390	530	210	480
BL-10	7.2Cr-14.5Ti	1110	250	400	400
BL-21	13.7Cr-4.8Ti	340	510	180	1150
BL-22	13.4Cr-5.1Ti	300	52	150	56
BL-23	12.9Cr-5.9Ti	400	490	280	1230
BL-24	13.5Cr-5.2Ti	1190	360	500	390
BL-25	14.4Cr-0.3Ti	390	64	120	<50
BL-26	14.1Cr-1.0Ti	560	86	140	<50
BL-40	10.9Cr-5.0Ti	470	80	90	270
BL-41	14.5Cr-5.0Ti	450	120	93	390
BL-43	9.2Cr-4.9Ti	230	31	100	340
BL-44	9.9Cr-9.2Ti	300	87	150	270
BL-47	4.1Cr-4.3Ti	350	220	200	870
BL-49	7.9Cr-5.7Ti	400	150	127	360
BL-54	5.1Cr-3.0Ti	480	82	133	655
BL-63	4.6Cr-5.1Ti	440	28	73	310
BL-62	3.1Ti-0.1Si	320	86	109	660
BL-27	3.1Ti-0.25Si	210	310	310	2500
BL-42	3.1Ti-0.5Si	580	190	140	5400
BL-45	2.5Ti-1Si	345	125	90	9900
QN74[a]	4.0Cr-4.1Ti	480	79	54	350
T87	4.9Cr-5.1Ti	380	89	109	545
832665[b]	3.8Cr-3.9Ti	310	85	80	783

[a]Contains ≈250 appm boron-10.

[b]500-kg production-scale heat, others, 15- to 30-kg laboratory heats.

Recently, a production-scale ingot of reference alloy V-4Cr-4Ti weighing ≈500 kg (Heat #832665 in Table 1) was melted and extruded successfully by essentially the same fabrication procedures as the laboratory-scale heats. In the fabrication of the production-scale ingot, particular attention was given to control of the following impurities: Nb and Mo (minimized to ensure low neutron activation); Cu (minimized to suppress Cu-rich vanadium oxycarbochlorides precipitation); Si (optimized to 400–1000 wppm to suppress swelling); O, N, and C (limited the combined concentration to <1000 wppm); S, P (minimized to avoid segregation to grain boundaries); and Cl, Ca, K, Mg, Na, and B (minimized to avoid formation of vanadium-based precipitates oxycarbochlorides, vanadates, and borides).

The procedures for extrusion, secondary fabrication, and conversion to plates and sheets of the production-scale heat of V-4Cr-4Ti were as follows:

1. Extrude ingot in stainless steel jacket at 1150°C into ≈65-mm-thick slab.
2. Subsequent warm rolling at 400°C to desired intermediate dimensions.
3. No more than 15% thickness reduction per each rolling step.
4. Less than 50% thickness reduction accumulated between annealings.
5. Anneal at 1050°C–1070°C for 2 h in high-vacuum furnace between rolling.
6. Anneal at 1050°C for 2 h in high-vacuum furnace only for selected final products thicker than ≈3.8 mm. Most of the products ≈3.8 mm or less in thickness were delivered in as-rolled condition and final-annealed in the laboratory at a desired temperature.

The results of chemical analyses, averaged over three measurements on 63-mm-thick extruded bars, are given in Table 2. For comparison, the chemical composition of the excellent ≈30-kg heat of V-4Cr-4Ti (ANL ID BL-47) is also given in the table.

Table 2. Chemical composition (impurities in wppm) of industrial-scale (500 kg) heat of V-4Cr-4Ti[a] and V raw stock used to melt ingot.

Heat ID	Material	Cr,	Ti,	Al	Fe	Mo	Nb	Cu	Si	O	N	C	S	P	Ca	Cl	B
820630	raw V	<100	<50	100	230	410	<50	<50	800	200	62	75	10	<30	–	<2	<5
832665	alloy	3.75%	4.16%	180	180	330	<50	<50	790	280	82	64	<10	<30	<10	<2	7
		3.72%	3.79%	190	220	350	50	<50	840	360	80	80	<10	<30	<10	<2	<5
		3.83%	3.80%	105	270	260	<50	<50	720	290	93	94	<10	<30	<10	<2	<5

[a]Determined from three different positions in the 64-mm-thick and 200-mm-wide extruded bar.

3. Specimens and Test Procedures

Test specimens were machined from cold- or warm-worked plates and sheets to investigate mechanical properties, swelling behavior, and microstructural characteristics. The machined test specimens were annealed mostly at 1000–1125°C for 1 h in high vacuum and exhibited an average grain size of ≈14–30 μm. Recrystallization was ≈60% complete after annealing at 1000°C for 1 h. However, some of the specimens were annealed at lower temperatures to investigate the effect of annealing on mechanical properties.

In the Ti-containing alloys, observed precipitates are usually Ti-based phases such as titanium oxycarbonitrides, titanium sulfides, or titanium phosphides.[6] However, in most of the alloys, the only secondary phase in the annealed specimen was spherical Ti(O,N,C) precipitates 300–500 nm in size, which is normally observed in titanium-containing vanadium alloys with O+N+C > 400 wppm.[6] Vanadium-base precipitates have been observed only rarely in V-Ti or V-Cr-Ti alloys.[6–8] Vanadium-base precipitates were observed only in alloys containing high levels of unusual impurities such as Cl, Ca, and Li, i.e., vanadium oxychlorides in V-5Cr-5Ti, which was melted with low-quality sponge Ti[7] and Ca-vanadate in unalloyed vanadium produced by the calcia-reduction process.[7] In an irradiated V-20Ti alloy rich in boron, Li-vanadate was also observed.[8]

Tensile specimens with a gauge length of 7.62 mm and a gauge width of 1.52 mm were machined from 1.0-mm-thick sheets. Tensile properties were determined at a strain rate of 0.0011 s^{-1} in flowing argon to minimize oxidation during testing. Creep properties were measured on similar tensile specimens. Impact properties were measured on blunt-notch and precracked Charpy specimens 3.33 x 3.33 x 25.4 mm in size (notch angle 30 or 45°, notch depth 0.61 mm, root radius 0.03 to 0.08 mm). In the Dynamic Helium Charging Experiment (DHCE), Charpy specimens could not be accommodated in the irradiation capsules because of limited space. Therefore, to extract crude information on the fracture behavior of the important alloy V-4Cr-4Ti irradiated in the DHCE, a TEM disk or a piece of broken tensile specimen was bent repeatedly until fracture in low-temperature baths of liquid nitrogen or mixtures of dry ice and acetone. However, results from this type of test on thin specimens should be considered only qualitative and limited in significance. Density was measured before and after irradiation using a standard TEM disk or a broken piece of a tensile specimen and research-grade CCl_4 solution. TEM disks were jet-thinned in a solution of 15% sulfuric acid-72% methanol-13% butyl cellosolve maintained at -5°C. TEM was conducted with a JEOL 100CX-II scanning transmission electron microscope (100 keV) or with a Philips CM-30 analytical electron microscope (200 keV).

4. Specimen Irradiation

The alloy specimens were irradiated in Li-bonded capsules in the Fast Flux Test Facility (FFTF), a sodium-cooled fast reactor, at 420-600°C up to ≈114 displacements per atom (dpa). The specimens were sealed in TZM/Mo capsules filled with 99.99%-enriched ^7Li during irradiation to prevent contamination by O, N, and C impurities dissolved in the sodium coolant of the FFTF. In this type of irradiation test, designed to simulate and investigate the effects of displacement damage on the physical and mechanical properties of the alloy, formation of appreciable levels of helium and tritium from ^6Li was avoided.

In contrast to the above type of irradiation test, the DHCE was designed to simulate and investigate the effects of simultaneous displacement damage and fusion-relevant helium generation (at a ratio of ≈4-5 appm helium/dpa) on the properties of the alloy. During irradiation in the DHCE, the fusion-relevant helium-to-dpa ratio is simulated realistically by utilizing transmutation of controlled amounts of ^6Li and predetermined amount of tritium-doped vanadium mother alloy immersed in ^6Li + ^7Li.[9,10] Table 3 gives a summary of postirradiation parameters determined from tensile and disk specimens of the V-4Cr-4Ti alloy irradiated in the DHCE, i.e., fast neutron fluence, dose, and helium and tritium contents measured shortly after the postirradiation tests.[9,10]

Table 3. Irradiation parameters of the DHCE and helium and tritium contents measured in V-4Cr-4Ti specimens

Capsule ID No.	Irradiation Temp. (°C)	Initial Tritium Charge (Ci)	Total Damage (dpa)	Measured Helium Content (appm)	Actual Helium to dpa Ratio (appm/dpa)	Measured Tritium Content (appm)
4D1	425	99	31	11.2-13.3	0.39	27
4D2	425	70	31	22.4-22.7	0.73	39
5E2	425	26	18	3.3-3.7	0.11	2
5D1	500	73.5	18	14.8-15.0	0.83	4.5
5E1	500	57	18	6.4-6.5	0.36	1.7
5C1	600	16.4	18	8.4-11.0	0.54	20
5C2	600	18	18	74.9-75.3	4.17	63

5. Baseline Tensile Properties

Yield and ultimate tensile strengths of unirradiated V-Cr-Ti alloys are shown in Figs. 1 and 2, respectively, as a function of temperature. Titanium and the combined contents of O, N, and C impurities in the four alloys were similar, i.e., 4-5 wt.% and 360-770 wppm,

respectively. Ti content of 4–5 wt.% in the ternary alloys was of particular interest primarily for creep strength and resistance to irradiation–induced swelling. Note that yield strengths of the alloys are nearly constant between 300 and 600°C. For all test temperatures, the yield and ultimate strengths increased monotonically with increased Cr content, indicating the predominant role of Cr on tensile strength of the alloy system.

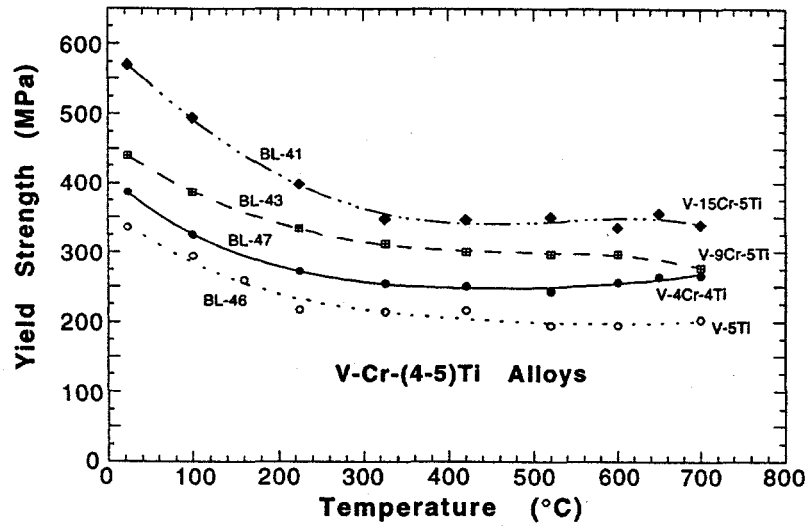

Fig. 1.

Yield strength of unirradiated V-Cr-(4–5)Ti alloys at 23°C–700°C.

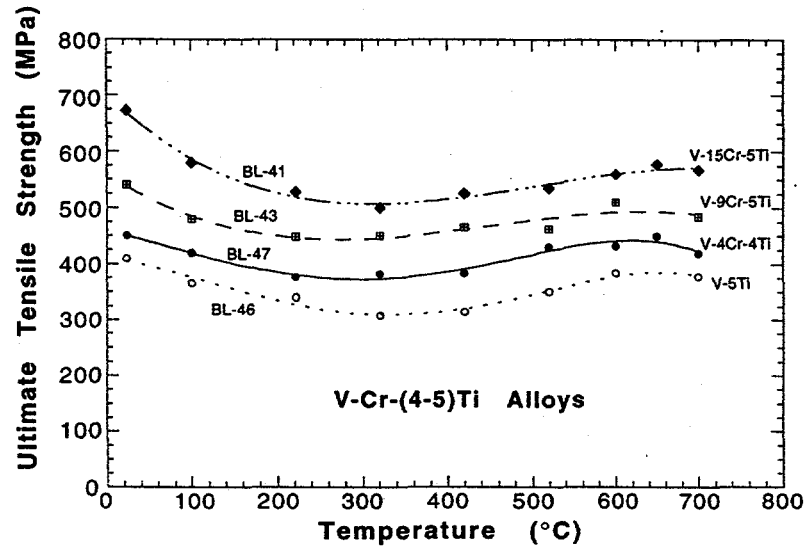

Fig. 2.

Ultimate tensile strength of unirradiated V-Cr-(4–5)Ti alloys at 23°C–700°C.

The yield strength of all alloys listed in Table 1 at room temperature and 420°C–600°C could be correlated well with combined content of Cr and Ti; this is shown in Fig. 3. Excessive alloying addition of Cr (≥6 wt.%) is not desirable from the standpoint of irradiation–induced degradation of material toughness. Likewise, excessive addition of Ti (≥9 wt.%) is not desirable from the standpoint of lower thermal creep resistance.

Tensile strength, ductility, and reduction–in–area of the reference alloy V–4Cr–4Ti are shown in Figs. 4–6, respectively. The alloy has been identified as the most promising candidate on the basis of its excellent resistance to irradiation–induced embrittlement, swelling, creep, and microstructural instability. Reduction–in–area of a similar alloy (V–5Cr–5Ti) is also shown in Fig. 6. On the basis of results in Figs. 4-6, tensile properties of

V-(4-5)Cr-(4-5)Ti alloys are excellent up to ≈650°C; above that temperature, tensile ductility decreases significantly.

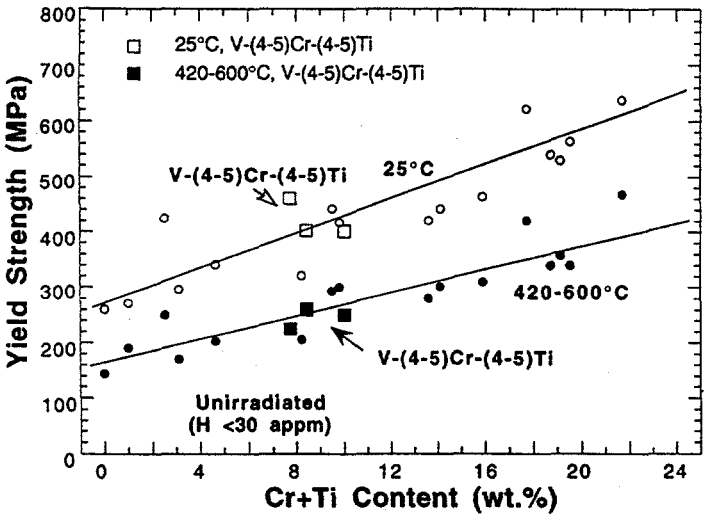

Fig. 3.

Yield strength of unirradiated V, V–Ti, V–Cr–Ti, and V–Ti–Si alloys at 25°C and 420°C–600°C as function of combined Cr and Ti content.

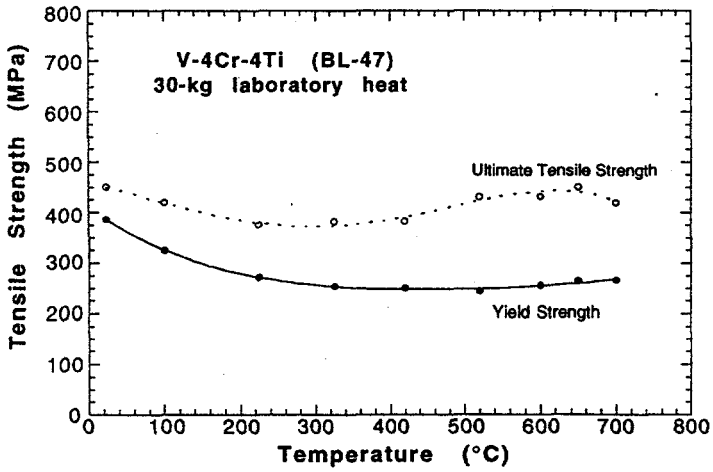

Fig. 4.

Yield and ultimate tensile strength of unirradiated reference alloy V-4Cr-4Ti at 23°C–700°C.

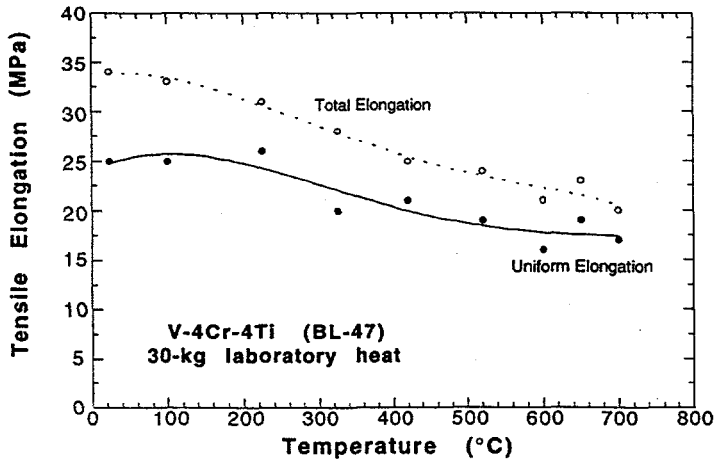

Fig. 5.

Uniform and total elongation of unirradiated reference alloy V-4Cr-4Ti at 23°C–700°C.

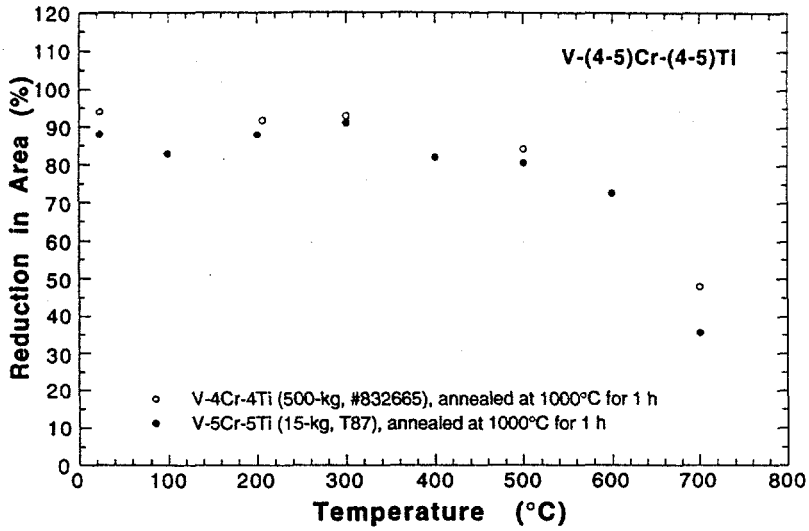

Fig. 6.

Reduction in area of unirradiated V-(4–5)Cr-(4–5)Ti alloys at 23°C–700°C.

6. Thermal Creep Properties

Stress-rupture life and steady-state creep rate of V-4Cr-4Ti and V-10Cr-5Ti have been determined in a carefully controlled vacuum environment at 600°C.[11] In Fig. 7, stress–rupture behavior of the reference alloy V–4Cr–4Ti is shown in Larsen-Miller plots. For comparison, similar properties of ferritic/martensitic and austenitic steels are also included in the figure. It is obvious that the creep strength of V-4Cr-4Ti is substantially superior to that of HT-9, Type 316 stainless steel, and V-20Ti. In particular, this difference in creep strength seems to be more pronounced when Larsen-Miller parameters are higher, i.e., at higher temperatures or longer times.

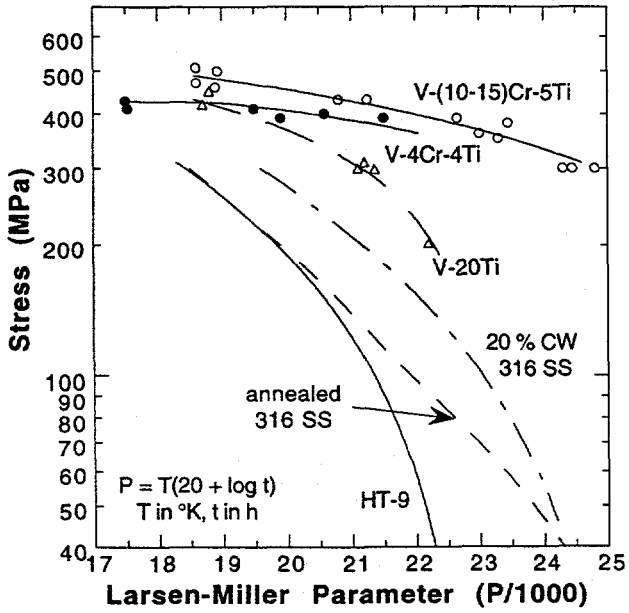

Fig. 7.

Larsen-Miller plots of creep strength of unirradiated V-4Cr-4Ti and ferritic and austenitic steels.

7. Baseline Impact Properties

Baseline impact properties of V, V–Ti, V–Ti–Si, and V–Cr–Ti alloys have been reported in Refs. 12 and 13. Examples of baseline impact data are shown in Figs. 8 and 9 for V–(9–15)Cr–5Ti and V–(4–5)Cr–(4–5)Ti alloys, respectively. Higher Cr increases the ductile–

brittle transition temperature (DBTT) of the ternary alloys significantly. For the high-Cr alloy V-15Cr-5Ti in Fig. 8, higher Si content appears to be conducive to higher DBTT (1150 wppm Si in BL-21 vs. 390 wppm in BL-24). In general, however, DBTT increases for increased contents of both Cr and Ti. This is shown in Fig. 10, in which DBTTs of V, V-Ti, V-Ti-Si, and V-Cr-Ti alloys are plotted as a function of combined concentrations of Cr and Ti. In the figure, data from a few alloys that were fabricated from low-quality raw materials and that contained abnormal vanadium-base precipitates were excluded. Alloys containing combined Cr and Ti contents of <10 wt.% did not exhibit DBTT for >-196°C.

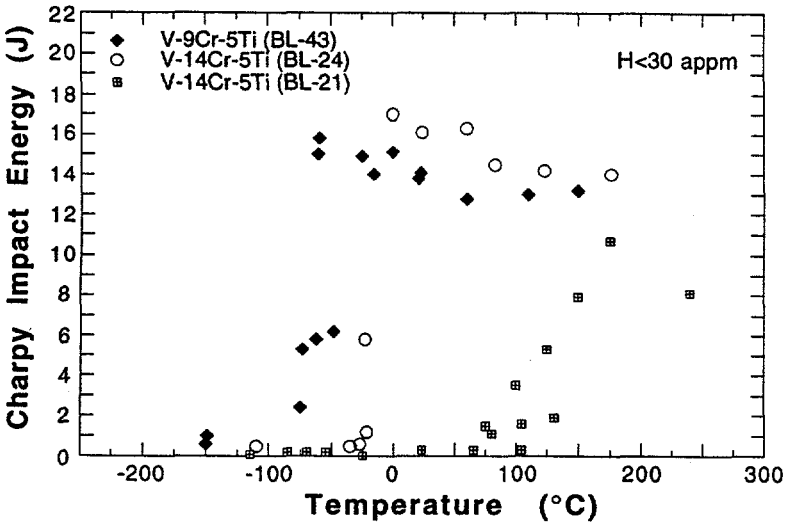

Fig. 8.

Impact properties of V-(9-15)Cr-5Ti alloys annealed at ≈1125°C for 1 h in high vacuum.

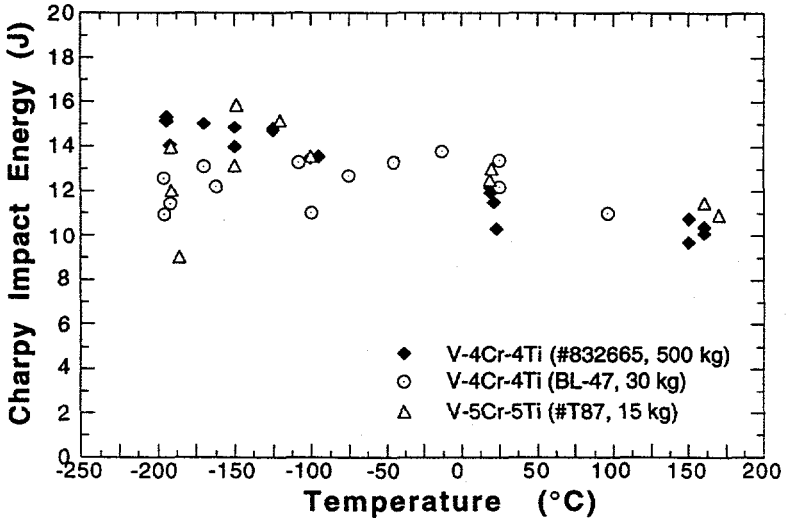

Fig. 9.

Impact properties of low-Cr ternary alloys V-(4-5)Cr-(4-5)Ti annealed at 1000°C for 1 h in high vacuum.

The 500-kg production-scale and 30-kg laboratory heats of the U.S. reference alloy V-4Cr-4Ti exhibited excellent impact properties; DBTT was no higher than -200°C and impact energies were greater than ≈10 J at all test temperatures (Fig. 9). The impact properties of the 15-kg laboratory heat of V-5Cr-5Ti were equally excellent.

However, impact properties of V-Cr-Ti alloys were found to be sensitive to final annealing condition. Results of extensive investigation on the effects of final annealing of V-(4-5)Cr-(4-5)Ti alloys have been reported in Refs. 14 and 15. In Fig. 11, effects of annealing on the impact properties of the 500-kg heat of V-4Cr-4Ti are shown. A summary of DBTT of V-4Cr-4Ti and V-5Cr-5Ti alloys is plotted in Fig. 12 as function of

annealing temperature. An important observation from the figure is that annealing at 1000°C for 1 h provides a sufficient tolerance of the reference alloy V–4Cr–4Ti to uncertainties in temperature and local chemical inhomogeneity. When annealed at the optimal temperature of 1000°C for 1 h in high vacuum, even precracked Charpy specimens of 30- and 500-kg heats of V–4Cr–4Ti retained ductile behavior at all temperatures ≥–196°C.[16] This is shown in Fig. 13.

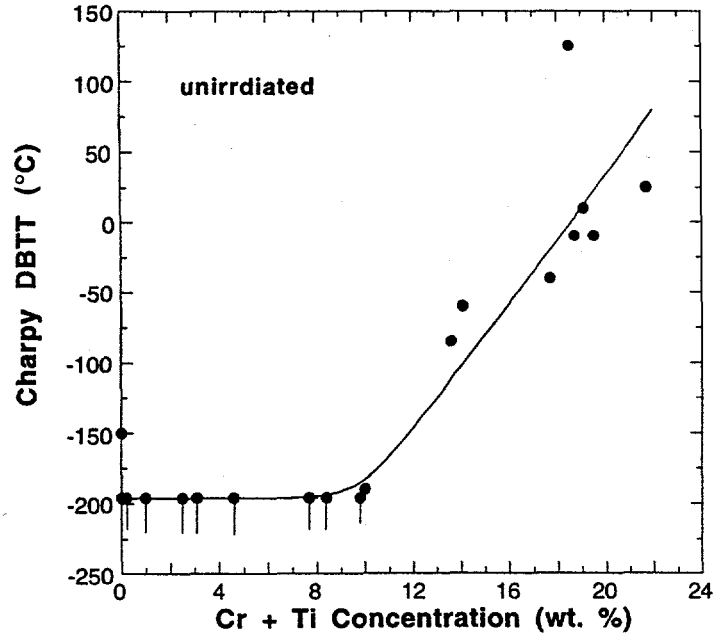

Fig. 10.

DBTT as function of combined Cr and Ti contents measured on one-third-size Charpy specimens of V, V–Ti, V–Ti–Si, and V–Cr–Ti alloys.

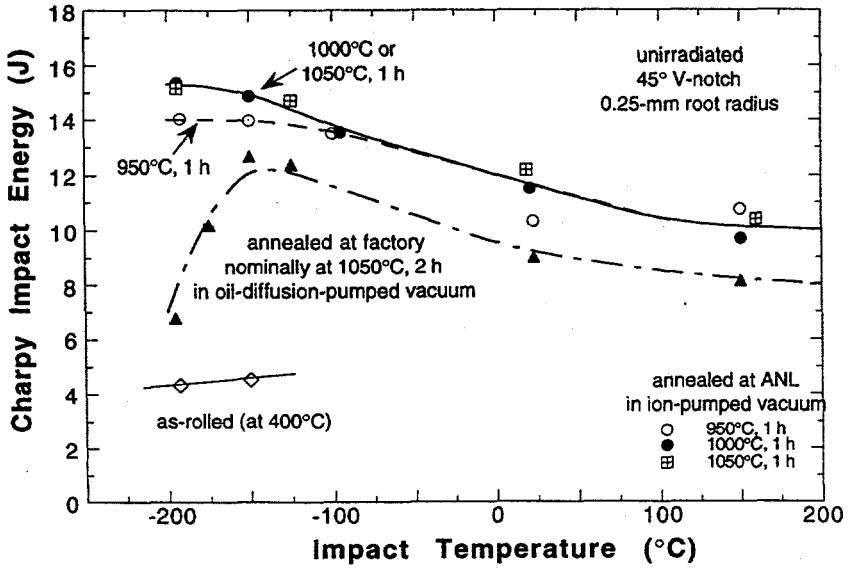

Fig. 11.

Impact properties of 500-kg heat of V–4Cr–4Ti after annealing for 1 h in high vacuum at various temperatures.

8. Density Change under Neutron Irradiation

Irradiation-induced density change and swelling behavior of V–4Cr–4Ti have been investigated after conventional neutron irradiation experiments (i.e., non-DHCEs).[8] V–Cr–Ti ternary alloys exhibited swelling (density change) maxima in the damage range of 30-70 dpa, as shown in Fig. 14, and swelling decreased on irradiation to higher dpa. Excellent resistance of the reference alloy V–4Cr–4Ti to swelling has been observed for up to ≈35 dpa in the conventional or DHCE irradiation.

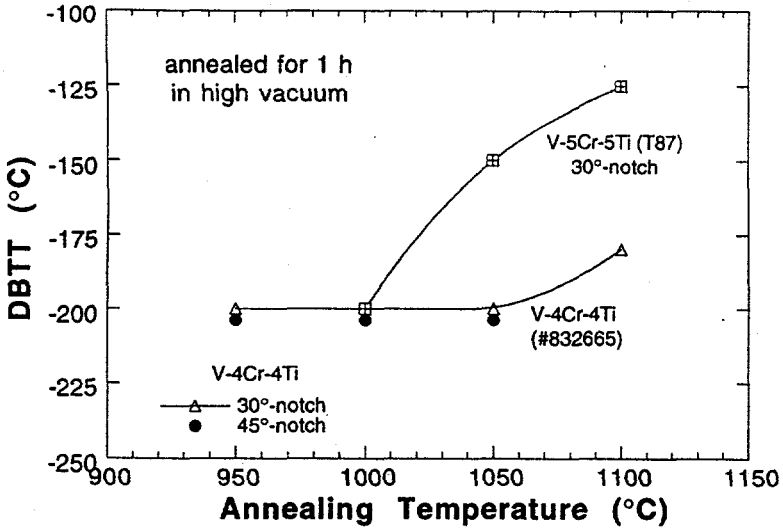

Fig. 12.

DBTT of V–4Cr–4Ti and V–5Cr–5Ti alloys as function of annealing temperature (1 h annealing in high vacuum).

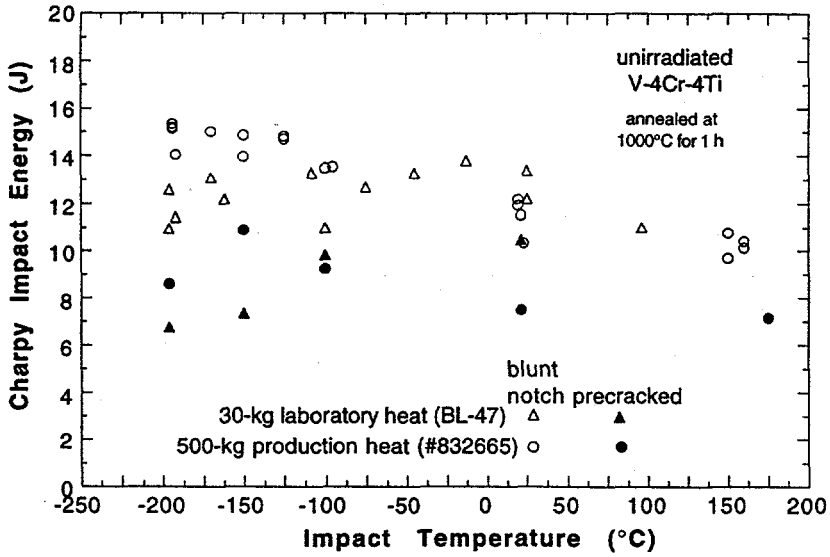

Fig. 13.

Impact properties of precracked and blunt-notch Charpy specimens of 30– and 500–kg heats of V–4Cr–4Ti annealed at 1000°C for 1 h in high vacuum.

High-density precipitation or clustering of ultrafine Ti_5Si_3 was found to be conducive to excellent swelling resistance of alloys containing Ti, and it was concluded that >4 wt.% Ti and 400-1000 wppm Si are desirable to effectively suppress swelling.[6] It appears convincing that as long as a vanadium–base alloy contains >4 wt.% Ti, swelling resistance is excellent, even in V–Fe–Ti alloys.

9. Microstructural Stability under Irradiation

The primary feature of microstructural evolution in the reference alloy V–4Cr–4Ti during non–DHCE irradiation (negligible helium generation) at 520 and 600°C was high-density formation of ultrafine Ti_5Si_3 precipitates, dislocation loops, and short dislocations. For irradiation at 420°C, precipitation of Ti_5Si_3 was negligible, and "black-dot" defects and dislocations were observed in significantly higher densities. Despite their extremely high densities, neither black-dot defects nor Ti_5Si_3 precipitates were overly detrimental to ductility and toughness of the alloy, yet they effectively suppress irradiation-induced swelling.

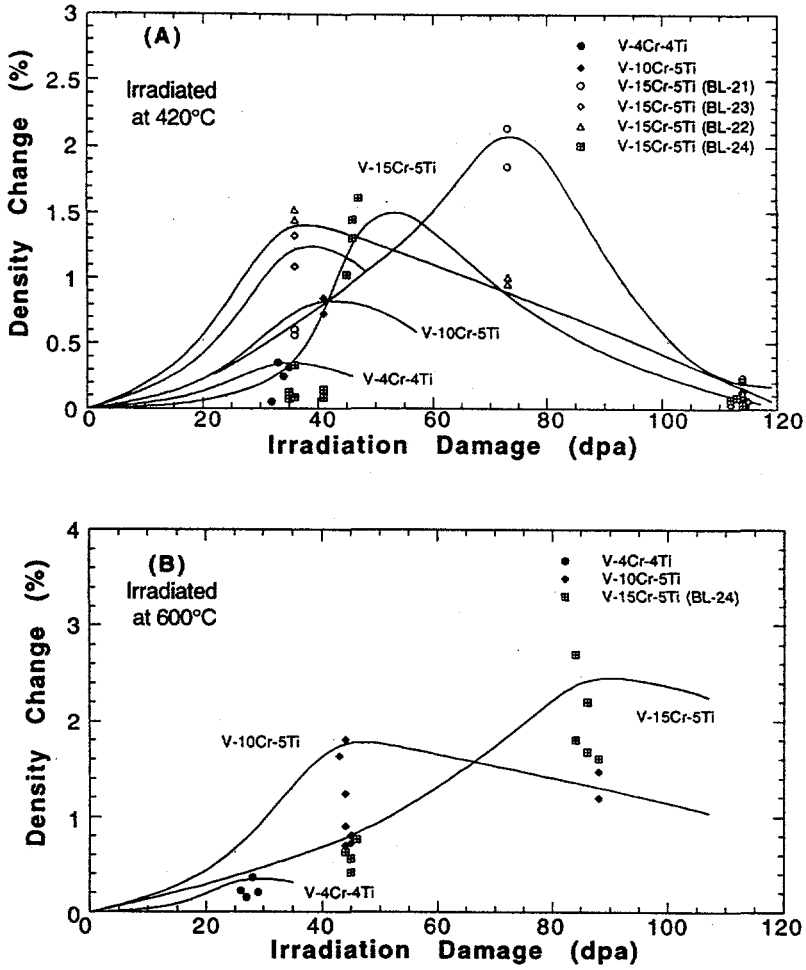

Fig. 14. Density change of V-Cr-Ti alloys as function of dose after irradiation at (A) 420 and (B) 600°C. Note the excellent resistance to swelling of V–4Cr–4Ti.

Thermally formed Ti(O,N,C) precipitates and irradiation–induced Ti_5Si_3 precipitates seemed to be stable during irradiation at 420–600°C. Unstable microstructural modifications that are likely to degrade mechanical properties significantly were not observed, e.g., irradiation-induced formation of fine oxides, carbides, nitrides, or chromium-rich clusters. Ti_5Si_3 did not precipitate during irradiation at 420°C but precipitated in similar density at 500–600°C in both DHCE and non–DHCE.

10. Effect of Neutron Irradiation on Tensile Properties

Effects of irradiation and test temperature on tensile properties of V–Cr–(4–5)Ti alloys, reported in Refs. 17 and 18, are given in Figs. 15–18. Effects of damage level (dpa) on the yield strength and the total elongation of the same alloys, determined after irradiation at 420°C, 520°C, and 600°C up to ≈120 dpa, are plotted in Figs. 19 and 20, respectively. Yield strength data show that the alloys undergo maximum irradiation–induced hardening on irradiation to ≈40 dpa; then this is followed by a decrease of hardening on further irradiation to >50 dpa. The exact mechanism of the decrease of hardening is not understood, although oxygen transfer from alloy matrix to lithium is speculated to be a factor. The tensile data also show that the total elongation of the alloys decreases with dose to ≈30 dpa and does not decrease further on irradiation to >50 dpa.

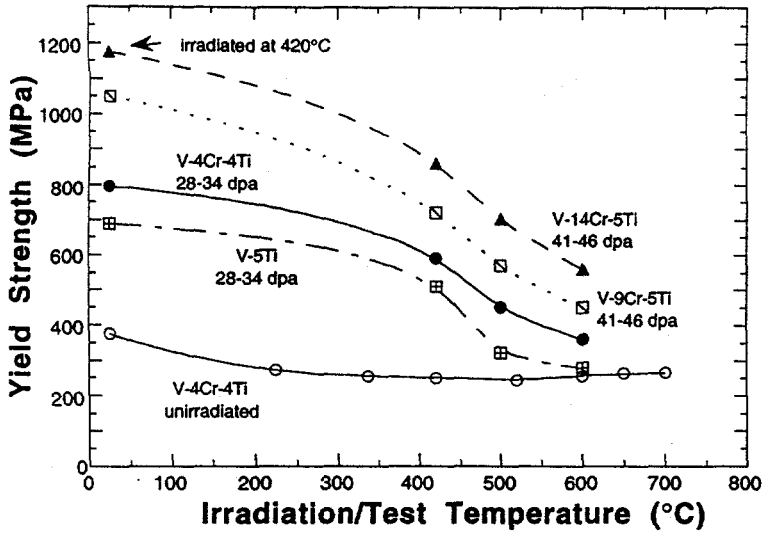

Fig. 15.
Yield strength of V-(0-15)Cr-(4-5)Ti alloys irradiated at 420°C-600°C to 24-46 dpa as function of irradiation and test temperature.

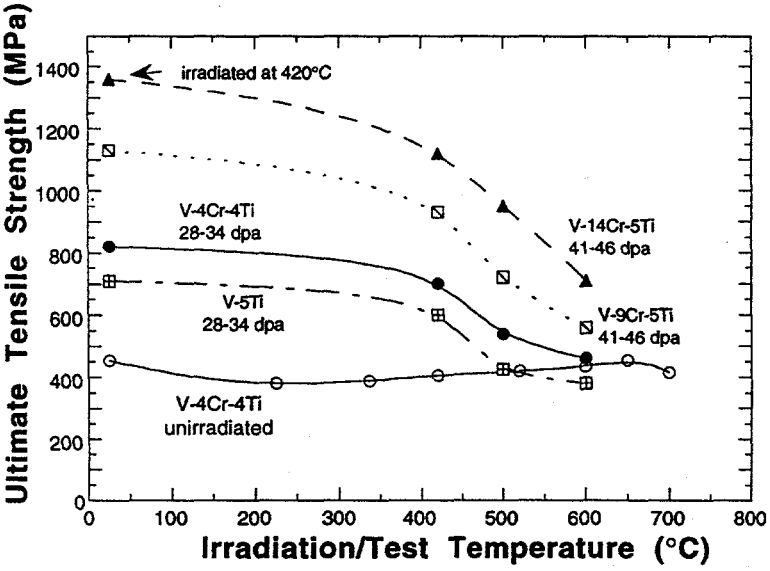

Fig. 16.

Ultimate tensile strength of V-(0-15)Cr-(4-5)Ti alloys irradiated at 420°C-600°C to 24-46 dpa as function of irradiation and test temperature.

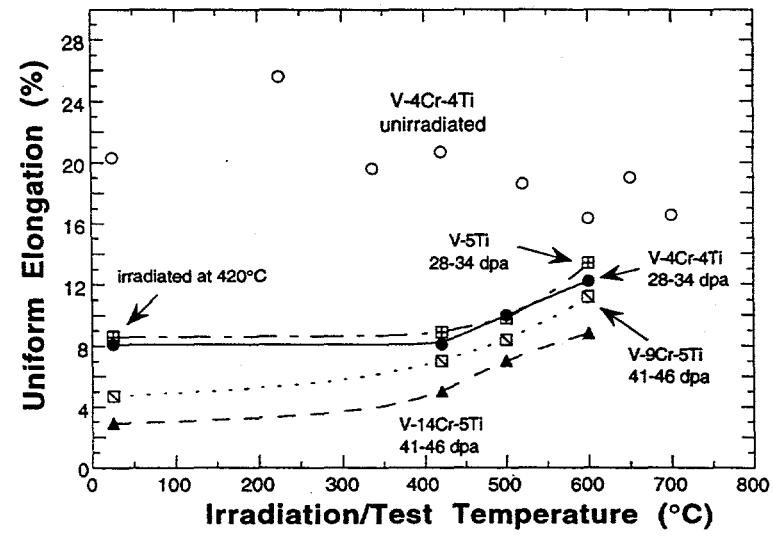

Fig. 17.

Uniform elongation of V-(0-15)Cr-(4-5)Ti alloys irradiated at 420°C-600°C to 24-46 dpa as function of irradiation and test temperature.

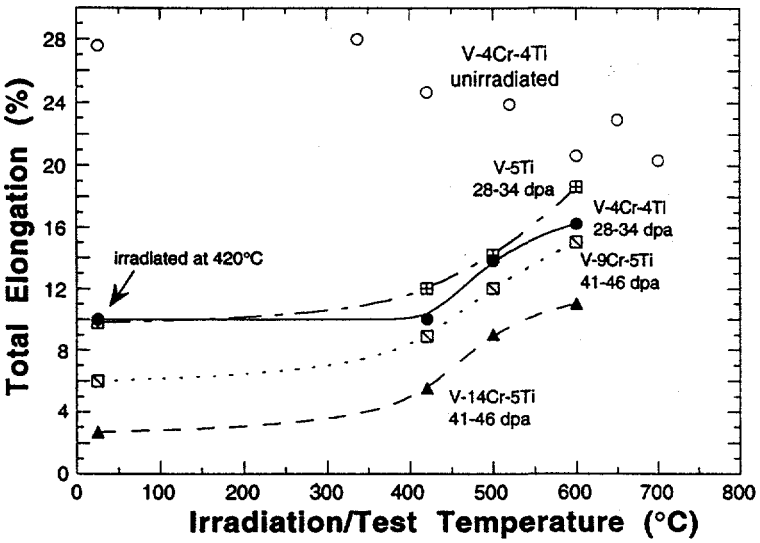

Fig. 18.

Total elongation of V–(0–15)Cr–(4–5)Ti alloys irradiated at 420°C–600°C to 24–46 dpa as function of irradiation and test temperature.

With the exception of V-14Cr-5Ti irradiated at 420°C, total elongation of the alloys exceeds ≈5% at the relatively high fluence of 1.7 x 10^{23} n/cm^2, or ≈100 dpa. The uniform elongation of the alloys, corresponding to ≈70% of the total elongation, exceeds ≈3%, showing a significant level of ductility retained after the high–dose irradiation.

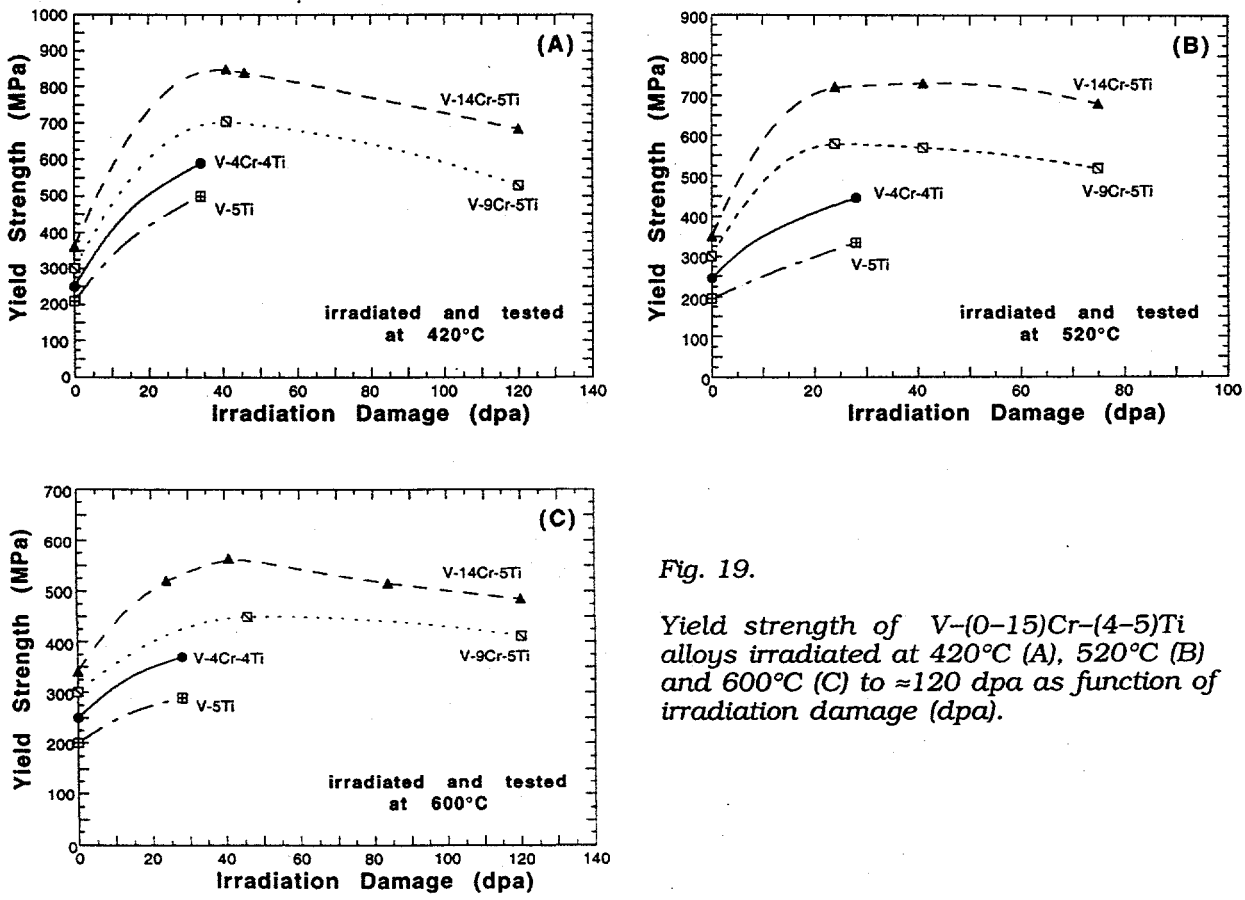

Fig. 19.

Yield strength of V–(0–15)Cr–(4–5)Ti alloys irradiated at 420°C (A), 520°C (B) and 600°C (C) to ≈120 dpa as function of irradiation damage (dpa).

Cr plays the most significant role in influencing the tensile properties of these alloys in both unirradiated and irradiated conditions. For irradiation at >600°C, irradiation-induced hardening of the alloy is insignificant. As expected, the effect of neutron irradiation on ductility is more pronounced at lower irradiation temperatures. However, after irradiation to 28–34 dpa at 420°C–600°C, the alloy still retained excellent ductility regardless of irradiation and test temperature, i.e., uniform and total elongation of ≈8 and 10%, respectively.

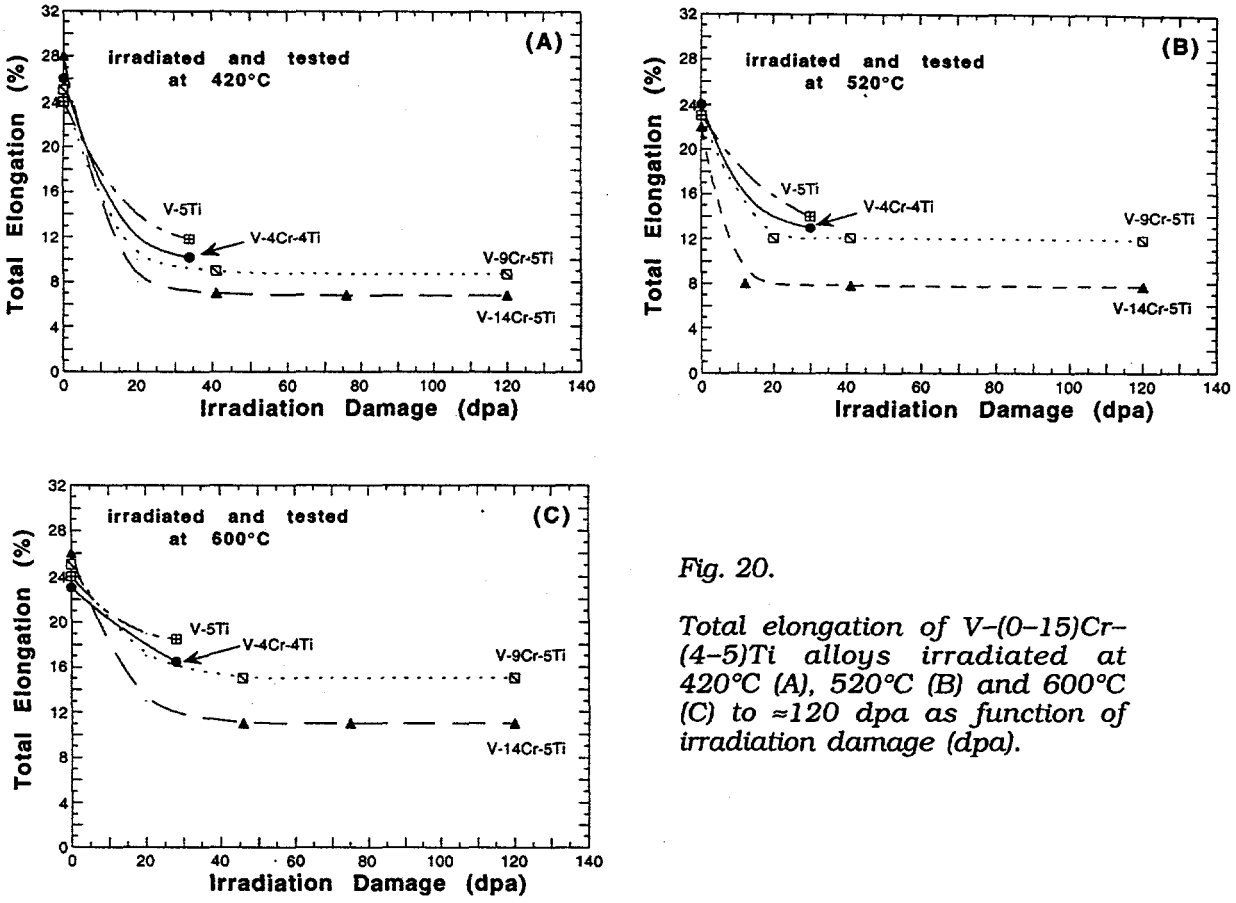

Fig. 20.

Total elongation of V–(0–15)Cr–(4–5)Ti alloys irradiated at 420°C (A), 520°C (B) and 600°C (C) to ≈120 dpa as function of irradiation damage (dpa).

11. Effect of Neutron Irradiation on Impact Properties

Impact data showing the effects of neutron irradiation relative to baseline impact properties of unirradiated specimens are shown in Figs. 21–23 for V–9Cr–5Ti, V–4Cr–4Ti, and V–5Ti, respectively.[19] Impact properties of V–4Cr–4Ti were virtually immune to neutron displacement damage, at least for the irradiation temperatures of 425°C–600°C. This is a remarkable property, considering the bcc structure of the alloy. Similar resistance to neutron displacement damage is also evident for V–5Ti, and to a lesser extent, for V–3Ti–1Si.[19] However, V–3Ti–Si family of alloys are not as excellent as the V–(4–5)Cr–(4–5)Ti alloys. Both V–3Ti–0.5Si and V–3Ti–1Si alloys seem to retain considerable hydrogen or tritium after irradiation in Li.

Effects of neutron irradiation on DBTT shift and upper-shelf energy were very significant for high–Cr alloys, e.g., V–9Cr–5Ti. Therefore, high–Cr alloys are simply unacceptable from the standpoint of irradiation embrittlement alone. To better define the effect of Cr, DBTTs of the V–Cr–(4–5)Ti alloys, determined before and after irradiation to 24–43 dpa at 420°C–600°C, have been plotted in Fig. 24 as a function of Cr concentration.

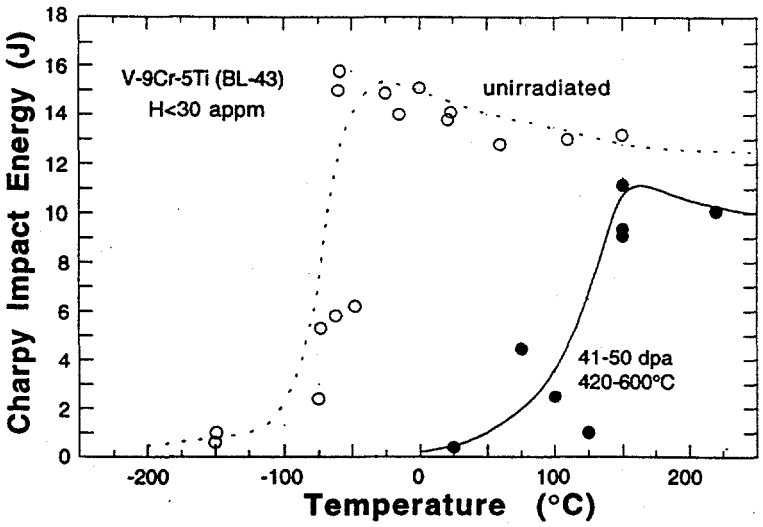

Fig. 21.

Impact properties of V–9Cr–5Ti (BL–43) before and after neutron irradiation in Li.

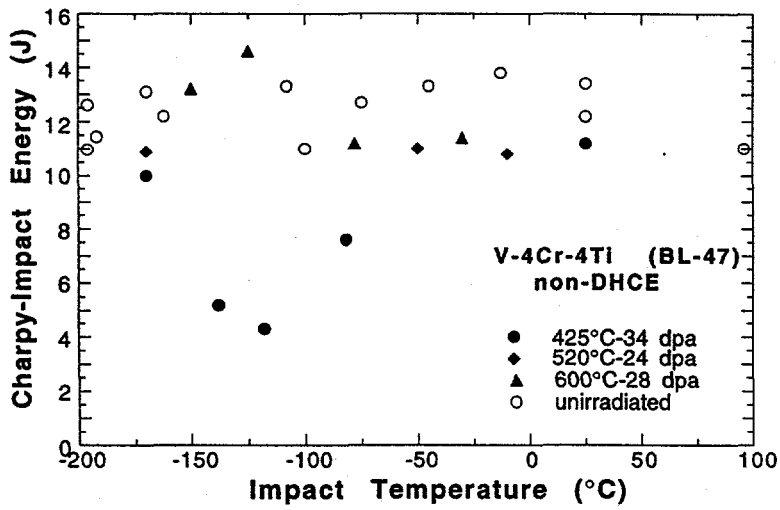

Fig. 22.

Impact properties and fracture behavior of V–4Cr–4Ti (BL–47) before and after neutron irradiation in Li.

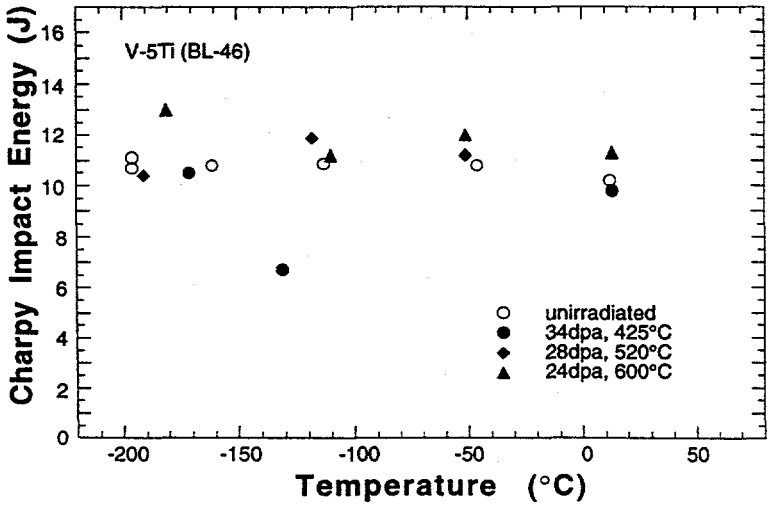

Fig. 23.

Impact properties of V–5Ti (BL–46) before and after neutron irradiation in Li.

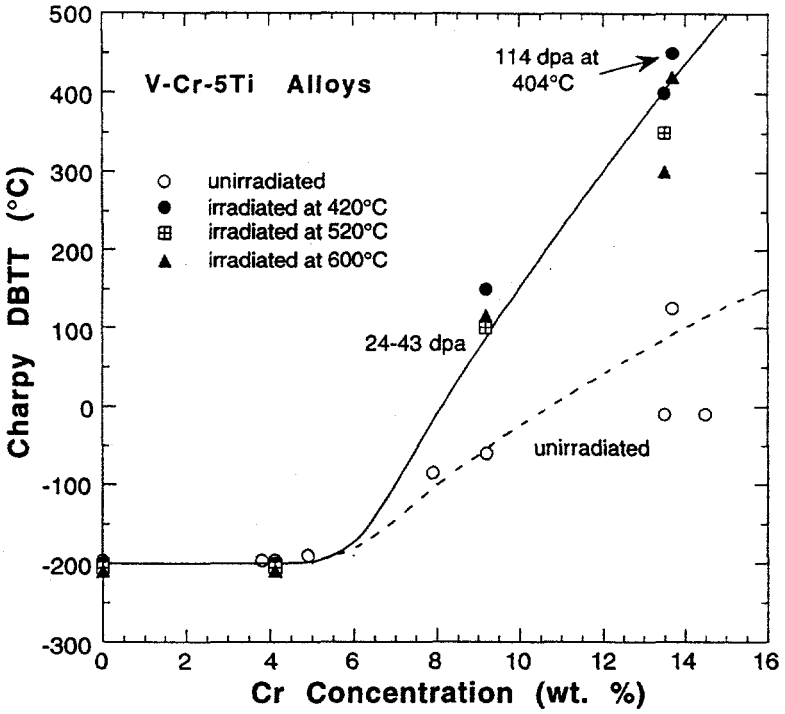

Fig. 24.

DBTT as function of Cr content measured on one-third-size Charpy specimens of V–Cr–5Ti alloys before and after irradiation to 24–43 dpa at 420°C–600°C.

The results in Fig. 24 clearly show that Cr content must be limited to <6 wt.% in order to ensure excellent impact properties (i.e., virtual immunity to irradiation embrittlement). Given a similar irradiation condition, DBTT shift is obviously more pronounced for increasing Cr content in the alloy. Although some effect of irradiation temperature is evident for high-Cr alloys, DBTT of V–Cr–5Ti alloys with Cr < 6 wt.% is so low (<–200°C) that the effect seems inconsequential for this range of irradiation temperature.

12. Effect of Dynamically Charged Helium on Void Swelling and Density

Effects of simultaneous neutron irradiation and helium generation were investigated for V–5Ti, V–4Cr–4Ti, V–3Ti–1Si, and V–8Cr–6Ti alloys in DHCE.[20] Tensile properties of V–4Cr–4Ti irradiated to 18–31 dpa at 425°C–600°C in DHCE (helium generation rate 0.4–4.2 appm He/dpa) are summarized in Fig. 25; to show helium effect directly, tensile properties determined after irradiation in non-DHCE[18] (negligible helium) and DHCE[20] with the same facility and by the same procedure are compared.

After irradiation to ≈31 dpa in either a DHCE or a non-DHCE, the four alloys retained significantly high ductilities, i.e., >8% uniform elongation and >10% total elongation. Although helium contents in the DHCE materials were relatively low, dependence of uniform and total elongation on irradiation and test temperature is in sharp contrast to similar results obtained on specimens in which helium atoms were produced by the tritium-trick method. In the latter approach, total elongation measured at room temperature and at 700–800°C was significantly lower than that measured at 500–600°C because of strong susceptibility to intergranular cracking associated with extensive formation of grain-boundary helium microcavities.[21] However, no intergranular fracture surface morphology was observed in the present tensile specimens irradiated in the DHCE and tested at 23–600°C. Tensile properties of the DHCE specimens measured at 420–600°C were essentially the same as those measured on non-DHCE specimens, showing that the effect of helium was insignificant. This is shown in Fig. 26, in which the ratio of total strain in specimens with and without helium is plotted as a function of irradiation and test temperature for the DHCE and tritium-trick experiments. In the tritium-trick

experiments, the deleterious effect of helium was significant at test temperatures of 25°C or >650°C. In contrast, the deleterious effect of helium was not observed in the DHCE.

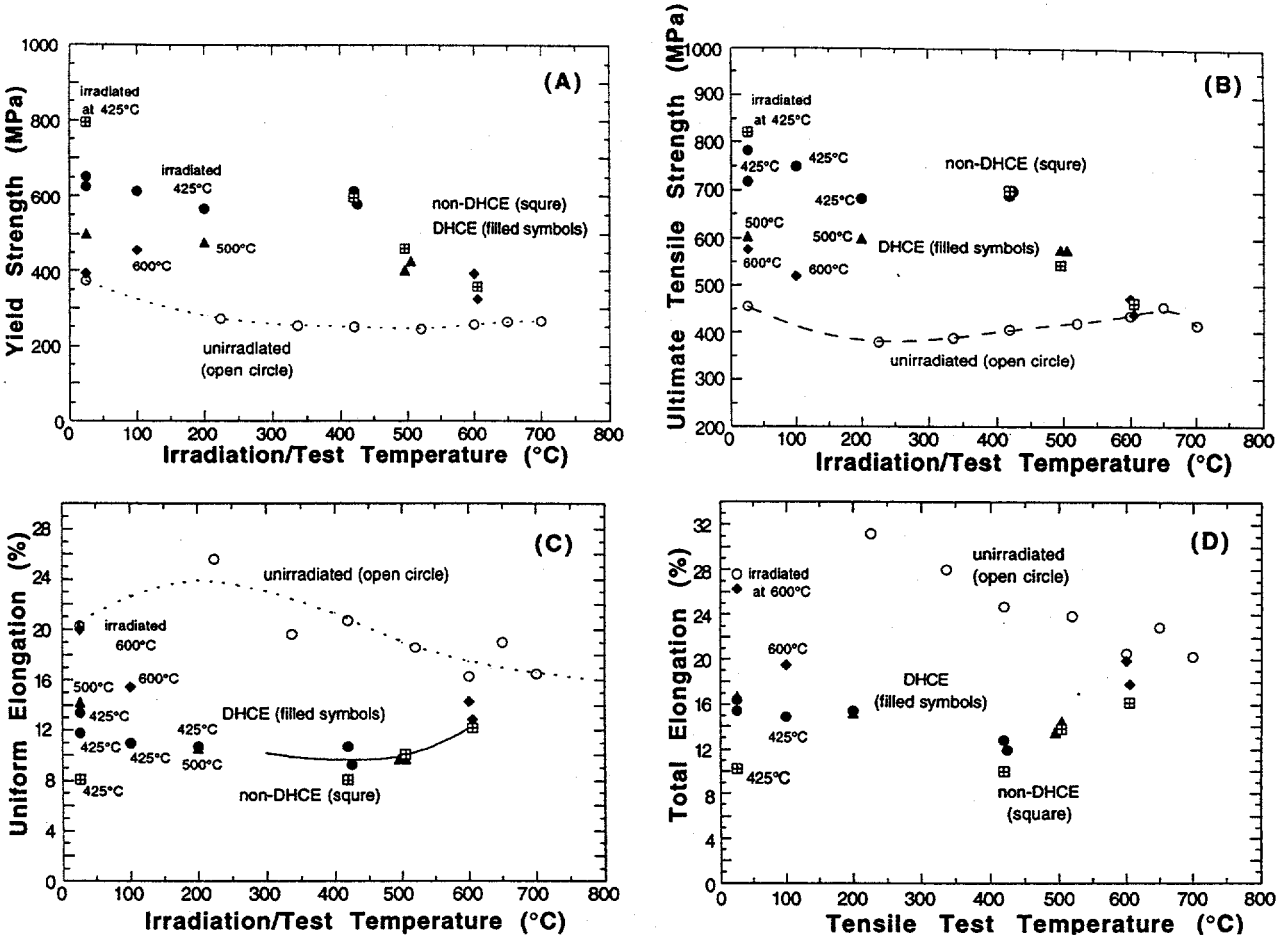

Fig. 25. Yield strength (A), ultimate tensile strength (B), uniform elongation (C), and total elongation (D) of V–4Cr–4Ti after irradiation at 420–600°C to 18–31 dpa in the DHCE (4–75 appm He) and in non-DHCE (<0.1 appm He).

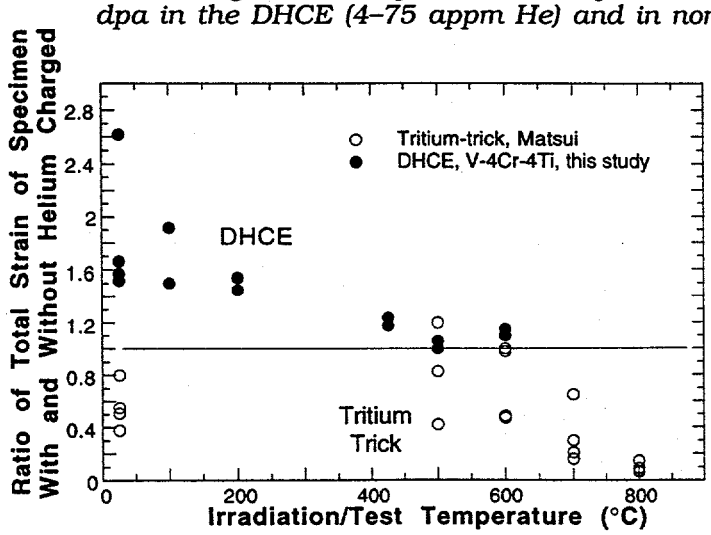

Fig. 26.

Ratio of total strain in specimens with and without helium as function of irradiation and test temperature. Results obtained from tritium–trick experiment and DHCE are shown for comparison.

Interestingly, ductilities of the DHCE specimens of all the four alloys irradiated at ≈420°C and measured at 20–200°C were higher than those of the non–DHCE specimens,

whereas strengths were lower. This indicates that a different type of hardening centers, stable at <250°C and absent in non–DHCE specimens, were produced during irradiation at in DHCE.

13. Effect of Helium on Fracture Behavior

Fracture behavior of the reference alloy V–4Cr–4Ti was investigated by multiple–bend test. Because no Charpy–impact specimens were irradiated in the DHCE, a TEM disk or a broken piece of a tensile specimen submerged in a low–temperature bath was bent repeatedly until fracture, and the cleavage morphology was then characterized quantitatively to determine ductile–brittle transition behavior. The percentage of ductile–fracture morphology is plotted as a function of test temperature in Fig. 27. Brittle cleavage at –196°C was more pronounced in specimens irradiated at 425°C. As in non–DHCE irradiation, no brittle behavior was observed at >–150°C for DHCE specimens for which the helium generation rate was ≈0.4–4.2 appm helium/dpa. Predominantly brittle–cleavage fracture morphologies were observed only at –196°C in some specimens irradiated to 31 dpa at 425°C. No intergranular fracture was observed.

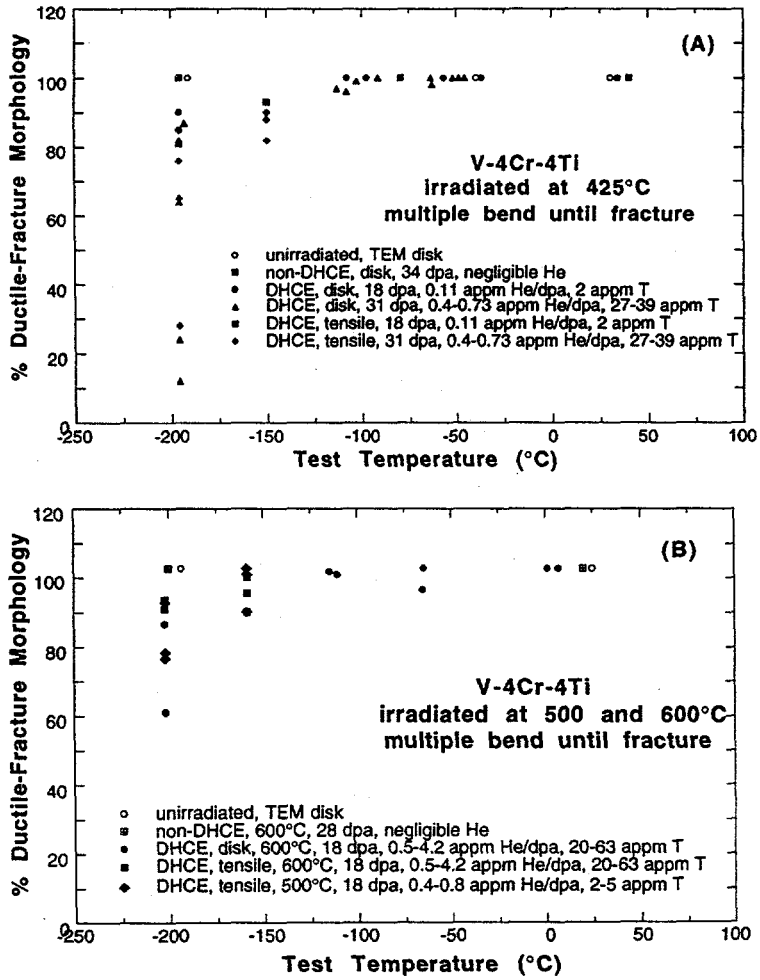

Fig. 27. Percent ductile–fracture morphology of V–4Cr–4Ti disk and tensile specimens irradiated at (A) 425°C and (B) 600°C and fractured by multiple bending.

14. Effect of Helium on Microstructure and Density

Voids or helium microcavities formed in the DHCE specimens were insignificant except for the unalloyed vanadium. For unalloyed vanadium specimens, in particular those irradiated to ≈31 dpa at 425°C, high-density helium bubbles (≈10 nm in diameter) were observed in the grain matrices. However, no evidence of grain-boundary coalescence of helium bubbles was observed; in contrast to the tritium-trick experiment, helium atoms produced dynamically in the presence of displacement damages in DHCE seem to form bubbles more or less uniformly within grains and on grain boundaries.[22]

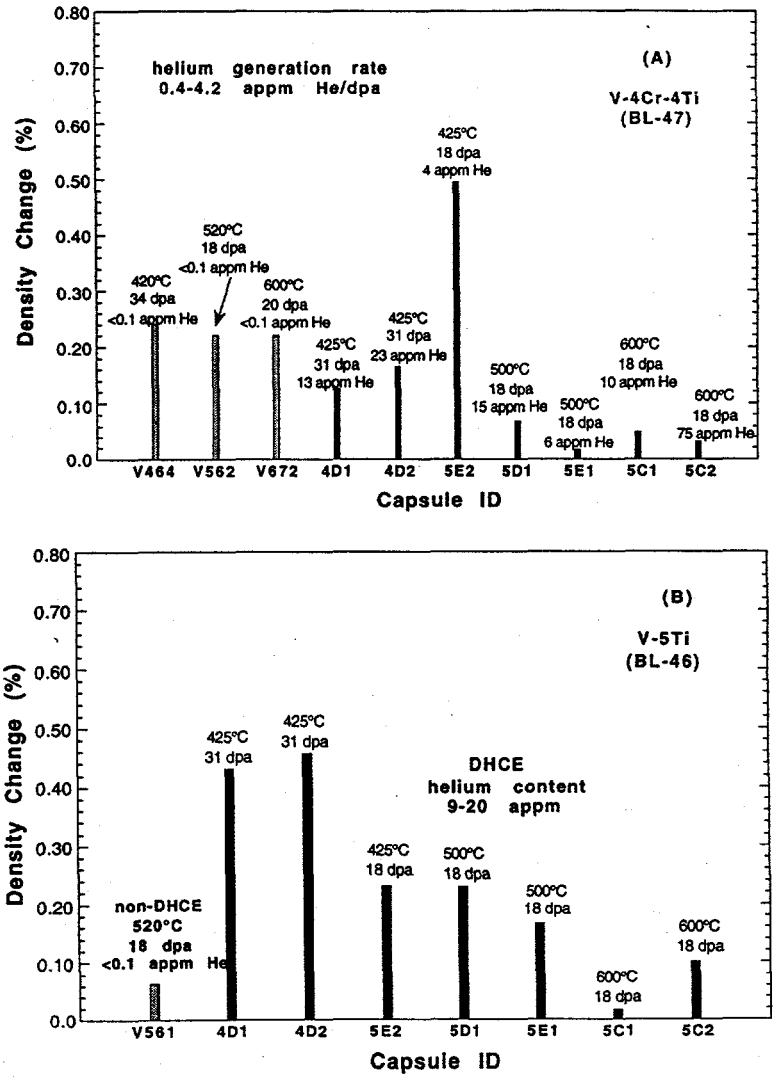

Fig. 28. Density decrease of (A) V-4Cr-4Ti and (B) V-5Ti after irradiation to 18-34 dpa at 420-600°C in DHCE (dark bars) and in non-DHCE (negligible helium) (light bars).

For irradiation at 500-600°C, only a few helium bubbles were observed on the Ti(O,N,C) precipitate interface in V-5Ti, V-4Cr-4Ti, V-8Cr-6Ti, and V-3Ti-1Si; virtually all of the dynamically produced helium atoms (helium generation rate 0.4-4.2 appm/dpa) in these alloys seem to have been trapped in the grain matrix without significant bubble

nucleation.[22] In V–4Cr–4Ti specimens irradiated at 425°C to ≈31 dpa, only a limited number of helium bubbles were distributed more or less uniformly within grains and on grain boundaries; no evidence of grain-boundary coalescence was observed. The absence of intergranular fracture morphology in any of the specimens irradiated in the DHCE seems to be consistent with the insignificant helium bubbles in either gain matrices or on grain boundaries. However, a more comprehensive data base is needed for irradiation temperatures <420°C to determine the effects of higher helium–dpa ratio.

Results of density measurements[23] on pieces of tensile specimens of V–4Cr–4Ti and V–5Ti are given in Fig. 28. For comparison, density changes determined for similar irradiation conditions in non–DHCEs are also shown in the figures. Density changes measured for the non–DHCE and DHCE specimens were low (<0.5 %). The small density change seems to be consistent with the negligible number density of voids or helium bubbles. Helium generation rates in the specimens were 0.4–4.2 appm He/dpa and there was no evidence of a significant effect of dynamically charged helium on density change of the several alloys investigated.[23]

It is likely that stable helium–vacancy–(O,N,C) complexes similar to those investigated by van Veen et al.[24] were present in the specimens irradiated at ≈420°C in DHCE during tensile tests at <220°C. In contrast, in specimens irradiated in non–DHCE under similar conditions, vacancies and impurities (such as O, N, and C) are not expected to form complexes in the absence of appreciable helium atoms. Rather, the impurity atoms in solution and vacancies or vacancy clusters will be scattered more or less randomly in interstitial and vacancy sites, respectively. Dislocation motion would be then more difficult under this condition, and ductility would thus be lower in the non–DHCE than in the DHCE specimens.

15. Welding Technology Development

Programs are being conducted to develop a welding procedure that can be applied to large–scale fusion–reactor structural components to be fabricated from vanadium–base alloys.[25–28] Although most of the current efforts are focused in gas-tungsten-arc (GTA), electron-beam (EB), and laser welding techniques, other procedures such as friction welding and resistance welding are also being developed. Initial results from investigations of GTA,[25] EB,[27] and laser[26,27] welds, however, indicate that toughness of the weldments is significantly inferior to that of base metal, and it appears that development of an acceptable welding procedure for application for large-scale field components is one of the most important challenges in the technology of vanadium-base alloys.

Impact properties of the laser and EB welds measured at –100 to 300°C are shown in Figs. 29 and 30, respectively.[27] Weld impact energies measured in as–welded condition and after postwelding annealing at 1000°C for 1 h in high vacuum are shown for comparison. Impact energy of the base metal is also shown. The DBTTs of the laser and EB welds were ≈80°C and ≈30°C, respectively, significantly shifted from the ≈–170°C DBTT of the base metal. However, excellent impact properties with DBTTs <–80°C could be restored in both the laser and EB welds by postwelding annealing at 1000°C for 1 h. Impact energies at <–80°C could not be measured because insufficient numbers of specimens were available. True DBTTs of the postwelding annealed laser and EB welds are probably as low as the DBTT of the base metal.

Apparently, a similar type of metallurgical process seems to occur during the postwelding annealing of laser and EB welds. Identification of this process appears, therefore, to be important in gaining an understanding of the mechanism causing the drastic improvement in impact toughness that is associated with the postwelding annealing. Microstructural characteristics were investigated to provide an understanding of the mechanism of the drastic improvement of impact toughness of welds following postwelding annealing at 1000°C.[28] Transmission electron microscopy (TEM) revealed that annealed weld zones were characterized by extensive networks of fine V(C,O,N) precipitates (NaCl type fcc structure, lattice constant 0.419 nm), which appear to clean away O, C, and N from grain matrices. This process is accompanied by simultaneous

annealing-out of the dense dislocations present in the weld fusion zone. The characteristic precipitate network imaged by optical microscopy and TEM is shown in Fig. 31. An example of the indexed diffraction patterns is shown in Fig. 32, in which one zone axis of vanadium and two zone axes of V(C, O, N) phase are operating. Indexed diffraction patterns obtained from the laser and EB welds showed that the precipitates formed in the two types of welds are the same V(C,O,N) phase. In EB welds, early development of the network of V(C,O,N) precipitates was observed even in as-welded state (i.e., without post-welding annealing), and this is probably reflected in the lower DBTT of the slower-cooled EB weld than that of the faster-cooled laser weld (i.e., ≈30°C vs. ≈80°C).

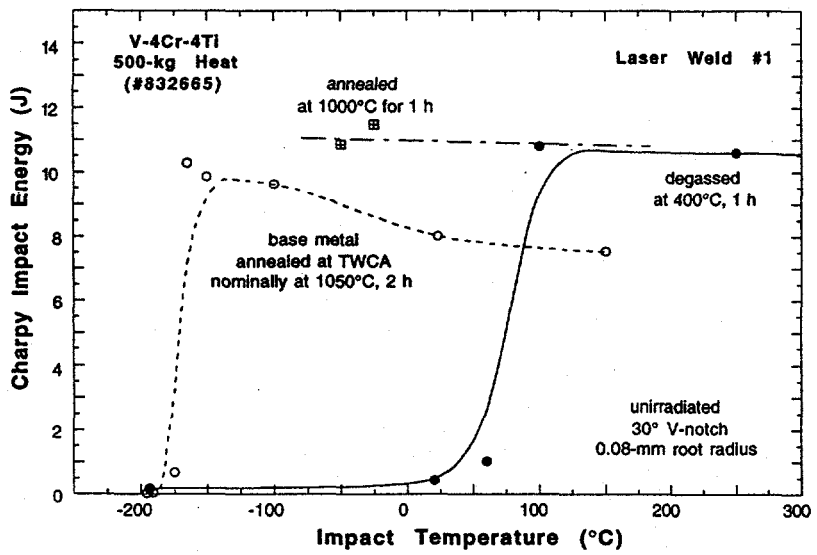

Fig. 29.

Impact properties of base metal and laser weld of V-4Cr-4Ti after annealing under various conditions.

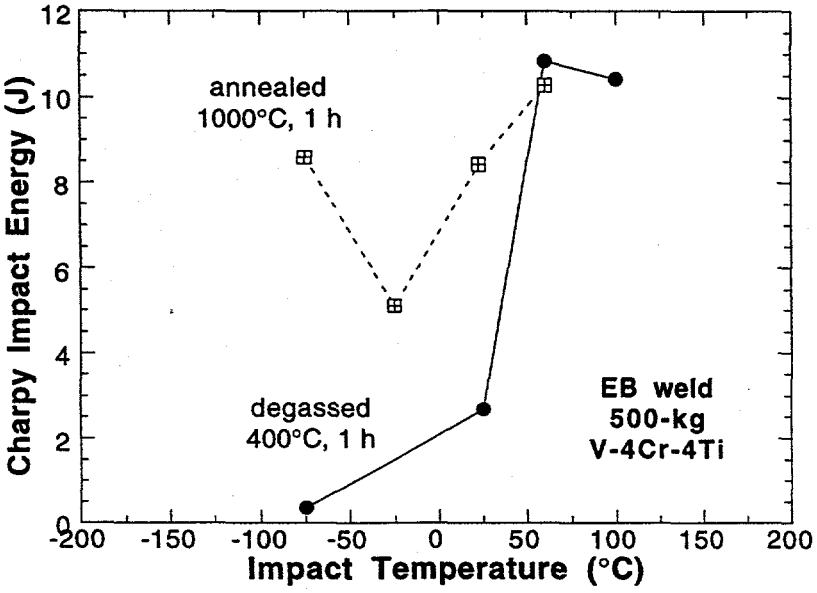

Fig. 30.

Impact properties of electron-beam weld of V-4Cr-4Ti after annealing at 400 and 1000°C.

Vanadium-base precipitates have been observed only rarely in V-Ti or V-Cr-Ti alloys. In the Ti-containing binary or ternary alloys, precipitates are usually Ti-based phases, such as titanium oxycarbonitrides, titanium sulfides, or titanium phosphides.[6] Vanadium-base precipitates were observed only in alloys containing high levels of unusual impurities such as Cl, Ca, and Li. Precipitation of V(C,O,N) seems to be preferred over precipitation of Ti(C,O,N) in a metastable structure such as the weld fusion zone. A laser or EB weld fusion

zone contains dense dislocations and higher levels of O, N, and C in the grain matrices following dissolution of Ti(O,N,C) during melting. It appears that a dense dislocation structure plays an essential role in the precipitation of V(C,O,N) in the welds. Under the same annealing condition at 1000°C, V(C,O,N) precipitates were not observed in the base metal, which is relatively free of dislocations and contains the normal Ti(O,N,C) precipitates. This seems to be additional evidence that high-density dislocations play an important role in the precipitation of (V(C,N,O) in the welds during postwelding annealing.

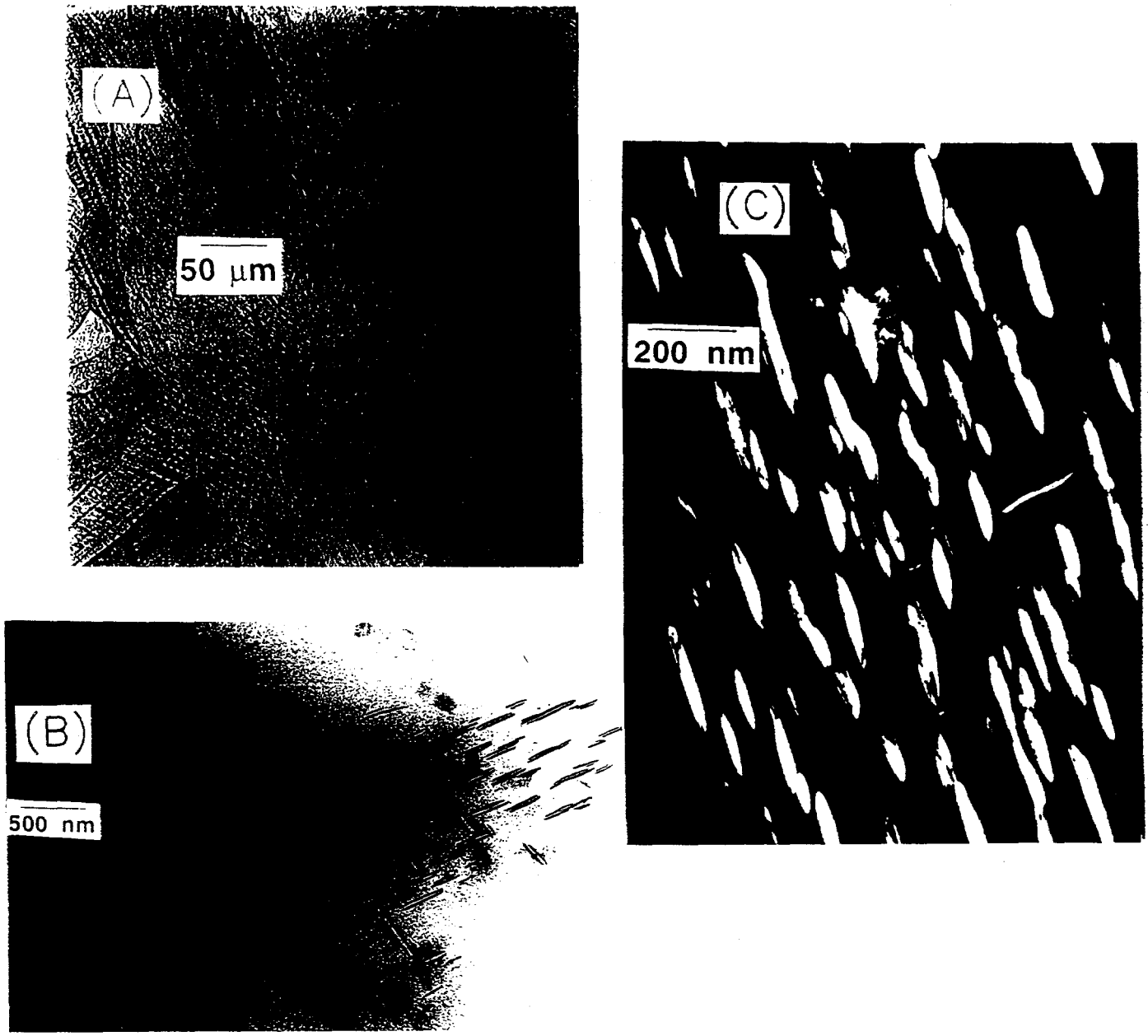

Fig. 31. Optical (A) and TEM bright- (B) and dark-field (C) photomicrographs of precipitates in laser weld fusion zone of V-4Cr-4Ti after postwelding annealing at 1000°C for 1 h.

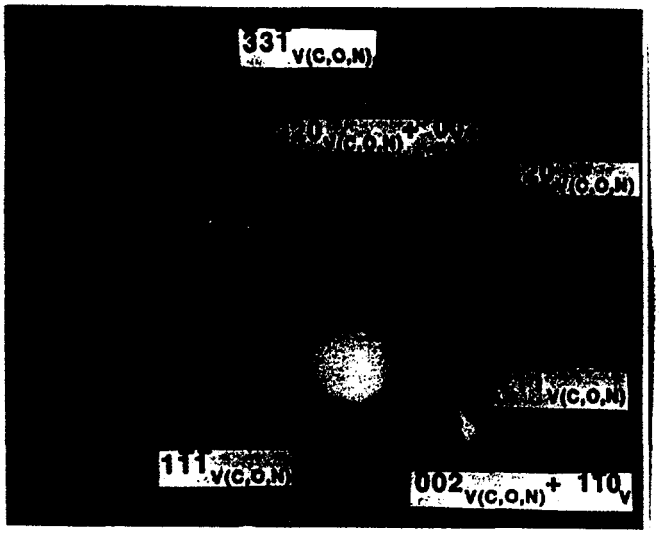

Fig. 32.
Indexed selected area diffraction pattern of laser weld fusion zone of V-4Cr-4Ti postwelding-annealed at 1000°C for 1 h. Reflections from (110) zone of vanadium and (110) and (123) zones of V(C,O,N) are visible.

Concentrations of O, C, and N were analyzed in EB welds. Three specimens of base metal and three specimens of EB weld were analyzed. These concentrations were compared with those measured on an extruded plate (64– mm thick) and the rolled base-metal plate (3.8– mm thick) from which the weld specimens were prepared. The base-metal plate was annealed in the factory nominally at ≈1050°C for 2 h and subsequently used in the present welding. Compared to the composition of the rolled and annealed base–metal plate, increase in O, N, and C in the EB welds was insignificant, that is, the average concentrations in wppm were: O 310, N 85, and C 80 in the extruded plate; O 466, N 27, and C 257 in the rolled base–metal plate; and O 517, N 28, and C 250 in the EB welds. Therefore, contamination by O, N, and C in the EB and laser welds appears to be at best a secondary factor in the large shifts in DBTT before and after welding.

It seems evident that the drastic improvement in impact toughness is a result of the simultaneous process of profuse formation of V(C,O,N) precipitates and annealing-out of the dense dislocations that occurs in the weld zone during postwelding annealing. The combined process seems to make grain matrices that are very low in O, C, and N and virtually free of dislocations and residual stress. Crack propagation through this type of microstructure would then be very difficult, leading to excellent impact toughness.

The precipitation kinetics of V(C,O,N) in the metastable structure of laser welds are believed to be strongly influenced by annealing temperature. Therefore, identification of the temperature of fastest precipitation kinetics in the time-temperature-transformation (TTT) curve will be important. This temperature is probably significantly higher than 1000°C, and the kinetics at that temperature seem to be fast. This can be deduced from observation of the early-stage development of the precipitate network in EB welds even without postwelding annealing. Controlled cooling of a laser weld would then be an attractive idea, in which the weld structure remains at the temperature of maximum precipitation kinetics for a reasonable period of time under reasonably practical conditions.

16. Summary and Conclusions

Vanadium-base alloys form an interesting system, especially in consideration of their unique potential for application in fusion energy devices. Significant progress has been achieved in the past decades in the development of vanadium-base alloys for application as structural materials in magnetic fusion reactors. In addition to the inherent advantages characteristic of vanadium-base alloys, V-(4-5)Cr-(4-5)Ti alloys — which were identified as the most promising — seem to be ideally suited for operation at 400-600°C in Li environment under fusion reactor conditions. Based on the extensive studies on baseline properties and irradiation testing in the present program, the following conclusions can be made:

1. Extensive investigation of baseline properties and irradiation performance of V, V-Cr,

V-Ti, V-Ti-Si, and V-Cr-Ti alloys has been conducted to screen and identify promising alloys. Irradiation performance was investigated by simulation experiments in fast reactors at 420-600°C in Li environments for up to ≈120 dpa with and without significant generation of helium (at a generation rate of up to 4.2 appm He/dpa) in the alloys. Based on the results of these investigations, V-(4-5)Cr-(4-5)Ti alloys were found to be most promising. A V-4Cr-4Ti alloy containing 500-1000 wppm Si and <1000 wppm O+N+C has been selected as the reference alloy.

2. Mechanical properties of V-(4-5)Cr-(4-5)Ti alloys are sensitive to impurities in the raw–material stocks or picked up during fabrication. An optimal fabrication process has been established to produce V-(4-5)Cr-(4-5)Ti alloys of excellent quality. Proper extrusion and annealing between rolling steps at the correct temperature and vacuum environment are important factors. This fabrication process has been demonstrated successfully by producing many small-scale heats of V-(3-6)Cr-(3-6)Ti alloys and a 500-kg industrial-scale heat of the reference alloy V-4Cr-4Ti.

3. Mechanical properties of V-(4-5)Cr-(4-5)Ti alloys are sensitive to final annealing. An annealing in high vacuum for 1–2 h at 1000°C produces the best mechanical properties in the alloys. When annealed properly, the reference alloy V-4Cr-4Ti exhibits excellent tensile and impact properties, while ensuring sufficient tolerance to effects of uncertainties in annealing temperature and compositional inhomogeneity.

4. V-4Cr-4Ti exhibits excellent thermal creep properties significantly superior to those of austenitic stainless steels or ferritic steels. However, irradiation-creep properties of the alloy with and without dynamic helium generation is not known.

5. Swelling of V-Ti and V-Cr-Ti alloys reaches its maxima at 30-70 dpa and decreases at higher damage levels. The swelling appears to be associated with irradiation-induced precipitation of titanium silicides, but the exact mechanism is not known.

6. Effects of neutron irradiation and dynamically charged helium on void swelling and density change of the reference alloy V–4Cr–4Ti were not significant; binary or ternary vanadium alloys containing >4 wt.% Ti seem to be inherently resistant to swelling.

7. Effects of neutron irradiation (in Li at 420-600°C) on tensile and impact properties of V-5Ti, V-4Cr-4Ti, and V-3Ti-1Si were not significant. Impact toughness of V-4Cr-4Ti was virtually immune to neutron displacement damage (up to ≈34 dpa under the irradiation conditions), and DBTT of the alloy was lower than ≈-190°C before and after irradiation.

8. Effects of dynamically charged helium and neutron damage on ductile–brittle transition temperature (DBTT) of the reference alloy V–4Cr–4Ti were determined after irradiation in the Dynamic Helium Charging Experiment (DHCE) in Li at 420-600°C. Helium effects on tensile properties, fracture behavior, and swelling of the reference alloy V-4Cr-Ti appear to be insignificant at up to ≈30 dpa and helium generation rate of 0.4-4.2 appm/dpa at 500-600°C. No grain-boundary coalescence of helium bubbles or intergranular fracture characteristic of tritium-trick experiment was observed. However, helium effects at helium generation rate of >2 appm/dpa at <450°C are not clear, and further investigation is necessary.

9. Development of an acceptable welding procedure for application for large-scale field components appears to be one of the most important challenges in the technology of vanadium-base alloys. Although most of the current efforts are focused in gas-tungsten-arc (GTA), electron-beam (EB), and laser welding techniques, other procedures such as friction welding and resistance welding are also being developed. Initial results from investigation on GTA, EB, and laser welds showed that toughness of the weldments is significantly inferior to that of base metal. However, postwelding annealing at 950-1000°C for 1-2 h in vacuum restored the toughness to a level

superior or comparable to that of the base metal. The drastic improvement in impact toughness is a result of the simultaneous process of profuse formation of V(C,O,N) precipitates and annealing-out of the dense dislocations that occurs in the weld zone during the postwelding annealing. The combined process seems to make grain matrices that are very low in O, C, and N and virtually free of dislocations and residual stress. It seems possible to produce weldments of excellent toughness through an innovative controlled cooling, in which the weld structure remains at the temperature of maximum precipitation kinetics V(C,O,N) for a reasonable period of time.

17. Unresolved Issues

In spite of the significant progress described in this paper, the industrial base and large-scale application of components fabricated from vanadium-base alloys are still in infant stage. Several important issues still remain unresolved, and significant efforts are needed to investigate the issues:

1. Development of reliable welding procedure that can be applied to fabricate large-scale components in the field.
2. Performance of welds under irradiation and helium and tritium generating conditions.
3. Helium effects on mechanical properties at high dose and high helium concentration, in particular at <450°C.
4. Low–temperature (200-400°C) irradiation performance in an Li environment.
5. Irradiation creep properties.
6. Fatigue and subcritical crack growth under fusion–relevant conditions.
7. Static and dynamic fracture toughness under end-of-life levels of neutron damage and helium generation.
8. Better understanding of the sensitivity of mechanical properties to impurities and fabrication procedure.
9. Establishment of optimal ranges of primary and minor impurities in base metal and weldments.

References

[1] T. Noda, F. Abe, H. Araki, and M. Okada, J. Nucl. Mater. 155-157 (1988) 581.

[2] R. Santos, J. Nucl. Mater. 155-157 (1988) 589.

[3] S. J. Piet, et al., J. Nucl. Mater. 141-143 (1986) 24.

[4] F. L. Yaggee, E. R. Gilbert, and J. W. Styles, J. Less-Comm. Met. 19 (1969) 39.

[5] D. L. Smith, B. A. Loomis, and D. R. Diercks, J. Nucl. Mater. 135 (1985) 125.

[6] H. M. Chung, B. A. Loomis, and D. L. Smith, in Effects of Radiation in Metals: 16th Intl. Symp., ASTM STP 1175, D. S. Gelles, R. K. Nanstad, and T. A. Little, eds., American Society for Testing and Materials, Philadelphia, 1993, pp. 1185–1120.

[7] H. M. Chung, J. Gazda, L. J. Nowicki, J. E. Sanecki, and D. L. Smith, in U.S. Department of Enmergy Fusion Reactor Materials Semiannual Report, DOE/ER-0313/15, 1994, pp. 207–218.

[8] H. M. Chung, B. A. Loomis, D. L. Smith, J. Nucl. Mater. 212–215 (1994) 804.

[9] H. M. Chung, B. A. Loomis, H. Tsai, L. Nowicki, D. E. Busch, and D. L. Smith, in Fusion Reactor Materials Semiannual Prog. Report, DOE/ER-0313/16, Oak Ridge National Laboratory, Oak Ridge, TN (1994), pp. 212–219.

[10] H. M. Chung, B. A. Loomis, H. Tsai, L. Nowicki, J. Gazda, and D. L. Smith, in Fusion Reactor Materials Semiannual Prog. Report, DOE/ER-0313/16, Oak Ridge National Laboratory, Oak Ridge, TN (1994), pp. 204–211.

[11] H. M. Chung, B. A. Loomis, D. L. Smith, J. Nucl. Mater. 212–215 (1994) 772.

[12] B. A. Loomis and D. L. Smith, J. Nucl. Mater. 179–181 (1991) 783.

[13] H. M. Chung, B. A. Loomis, D. L. Smith, in ANL/FPP/TM–287, ITER/US/95/IV MAT–10, Argonne National Laboratory, 1995, p. 11.

[14] H. M. Chung, L. Nowicki, J. Gazda, and D. L. Smith, in Fusion Reactor Materials Semiannual Prog. Report, DOE/ER-0313/17, Oak Ridge National Laboratory, Oak Ridge, TN (1994) 183.

[15] H. M. Chung, L. Nowicki, D. Busch, and D. L. Smith, in Fusion Reactor Materials Semiannual Prog. Report, DOE/ER-0313/17, Oak Ridge National Laboratory, Oak Ridge, TN (1994), 259.

[16] H. M. Chung, L. Nowicki, and D. L. Smith, in Fusion Reactor Materials Semiannual Prog. Report, DOE/ER-0313/17, Oak Ridge National Laboratory, Oak Ridge, TN (1994) 253.

[17] B. A. Loomis, L. J. Nowicki, and D. L. Smith, in Fusion Reactor Materials Semiannual Prog. Report, DOE/ER-0313/15, Oak Ridge National Laboratory, Oak Ridge, TN (1994), 219.

[18] B. A. Loomis, L. J. Nowicki, and D. L. Smith, J. Nucl. Mater., 212–215 (1994) 790.

[19] B. A. Loomis, H. M. Chung, L. J. Nowicki, and D. L. Smith, J. Nucl. Mater., 212–215 (1994) 799.

[20] H. M. Chung, B. A. Loomis, L. Nowicki, and D. L. Smith, in Fusion Reactor Materials Semiannual Prog. Report, DOE/ER-0313/19, Oak Ridge National Laboratory, Oak Ridge, TN (1996) 77.

[21] H. Matsui, M. Tanaka, M. Yamamoto, and M. Tada, J. Nucl. Mater. 191-194 (1992) 919.

[22] H. M. Chung, L. Nowicki, J. Gazda, and D. L. Smith, in Fusion Reactor Materials Semiannual Prog. Report, DOE/ER-0313/17, Oak Ridge National Laboratory, Oak Ridge, TN (1995) 211.

[23] H. M. Chung, T. M. Galvin, and D. L. Smith, in Fusion Reactor Materials Semiannual Prog. Report, DOE/ER-0313/19, Oak Ridge National Laboratory, Oak Ridge, TN (1996) 83.

[24] A. van Veen, H. Eleveld, and M. Clement, J. Nucl. Mater. 212–215 (1994), 287.

[25] J. F. King, G. M. Goodwin, and D. J. Alexander, in Fusion Reactor Materials Semiannual Prog. Report, DOE/ER-0313/17, Oak Ridge National Laboratory, Oak Ridge, TN (1995) 152.

[26] R. V. Strain, K. H. Leong, and D. L. Smith, in Fusion Reactor Materials Semiannual Prog. Report, DOE/ER-0313/19, Oak Ridge National Laboratory, Oak Ridge, TN (1996) 3.

[27] H. M. Chung, R. V. Strain, H.–C. Tsai, J.–H. Park, and D. L. Smith, in Fusion Reactor Materials Semiannual Prog. Report, DOE/ER-0313/20, Oak Ridge National Laboratory, Oak Ridge, TN (1996), in press.

[28] H. M. Chung, J.–H. Park, J. Gazda, and D. L. Smith, in Fusion Reactor Materials Semiannual Prog. Report, DOE/ER-0313/20, Oak Ridge National Laboratory, Oak Ridge, TN (1996), in press.